Atmos. Chem. Phys., 21, 17099–17114, 2021 https://doi.org/10.5194/acp-21-17099-2021 © Author(s) 2021. This work is distributed under the Creative Commons Attribution 4.0 License.





Chemical composition of nanoparticles from α -pinene nucleation and the influence of isoprene and relative humidity at low temperature

Lucía Caudillo¹, Birte Rörup², Martin Heinritzi¹, Guillaume Marie¹, Mario Simon¹, Andrea C. Wagner³, Tatjana Müller¹,⁴, Manuel Granzin¹, Antonio Amorim⁵, Farnoush Ataei⁶, Rima Baalbaki², Barbara Bertozzi², Zoé Brasseur², Randall Chiu³, Biwu Chu², Lubna Dada³, Jonathan Duplissy²,9, Henning Finkenzeller³, Loïc Gonzalez Carracedo¹⁰, Xu-Cheng He², Victoria Hofbauer¹¹, Weimeng Kong¹²,¹³, Houssni Lamkaddam³, Chuan P. Lee³, Brandon Lopez¹¹, Naser G. A. Mahfouz¹¹, Vladimir Makhmutov¹⁴,²⁶, Hanna E. Manninen¹⁵, Ruby Marten³, Dario Massabò¹⁶, Roy L. Mauldin¹¹,¹¹¹, Bernhard Mentler¹³, Ugo Molteni³,²,0,²¹, Antti Onnela¹⁵, Joschka Pfeifer¹⁵, Maxim Philippov¹⁴, Ana A. Piedehierro²², Meredith Schervish¹¹, Wiebke Scholz¹³, Benjamin Schulze¹², Jiali Shen², Dominik Stolzenburg², Yuri Stozhkov¹⁴, Mihnea Surdu³, Christian Tauber¹⁰, Yee Jun Tham², Ping Tian²³, António Tomé²⁴, Steffen Vogt², Mingyi Wang¹¹, Dongyu S. Wang³, Stefan K. Weber¹⁵, André Welti²², Wang Yonghong², Wu Yusheng², Marcel Zauner-Wieczorek¹, Urs Baltensperger³, Imad El Haddad³, Richard C. Flagan¹², Armin Hansel¹8,¹9, Kristina Höhler², Jasper Kirkby¹,¹5, Markku Kulmala²,9,25, Katrianne Lehtipalo²,2², Ottmar Möhler², Harald Saathoff², Rainer Volkamer³, Paul M. Winkler¹⁰, Neil M. Donahue¹¹, Andreas Kürten¹, and Joachim Curtius¹

University of Helsinki, 00014 Helsinki, Finland

¹Institute for Atmospheric and Environmental Sciences, Goethe University Frankfurt, 60438 Frankfurt am Main, Germany

²Institute for Atmospheric and Earth System Research (INAR)/Physics, Faculty of Science,

³Department of Chemistry & CIRES, University of Colorado Boulder, Boulder, CO 80309-0215, USA

⁴Atmospheric Chemistry Department, Max Planck Institute for Chemistry, 55128 Mainz, Germany

⁵CENTRA and FCUL, University of Lisbon, 1749-016 Lisbon, Portugal

⁶Leibniz Institute for Tropospheric Research, 04318 Leipzig, Germany

⁷Institute of Meteorology and Climate Research, Karlsruhe Institute of Technology,

⁷⁶³⁴⁴ Eggenstein-Leopoldshafen, Germany

⁸Laboratory of Atmospheric Chemistry, Paul Scherrer Institute, 5232 Villigen, Switzerland

⁹Helsinki Institute of Physics (HIP)/Physics, Faculty of Science, University of Helsinki, 00014 Helsinki, Finland

¹⁰Faculty of Physics, University of Vienna, 1090 Vienna, Austria

¹¹Center for Atmospheric Particle Studies, Carnegie Mellon University, Pittsburgh, PA 15213, USA

¹²Division of Chemistry and Chemical Engineering, California Institute of Technology, Pasadena, CA 91125, USA

¹³California Air Resources Board, Sacramento, CA 95814, USA

¹⁴Lebedev Physical Institute, Russian Academy of Sciences, 119991, Moscow, Russia

¹⁵CERN, 1211 Geneva, Switzerland

¹⁶Dipartimento di Fisica, Università di Genova and INFN, 16146 Genoa, Italy

¹⁷Department of Atmospheric and Oceanic Sciences, University of Colorado Boulder, Boulder, CO 80309, USA

¹⁸Institute for Ion and Applied Physics, University of Innsbruck, 6020 Innsbruck, Austria

¹⁹Ionicon Analytik GmbH, 6020 Innsbruck, Austria

²⁰Forest Dynamics, Swiss Federal Institute for Forest, Snow and Landscape Research, 8903 Birmensdorf, Switzerland

²¹Department of Chemistry, University of California, Irvine, CA 92697, USA

²²Atmospheric Composition Unit, Finnish Meteorological Institute, 00560 Helsinki, Finland

²³Beijing Weather Modification Office, 100089 Beijing, China

²⁴IDL, Universidade da Beira Interior, R. Marquês de Ávila e Bolama, 6201-001 Covilhã, Portugal

Correspondence: Lucía Caudillo (lucia.caudillo@iau.uni-frankfurt.de) and Joachim Curtius (curtius@iau.uni-frankfurt.de)

Received: 16 June 2021 – Discussion started: 7 July 2021

Revised: 15 October 2021 - Accepted: 17 October 2021 - Published: 25 November 2021

Abstract. Biogenic organic precursors play an important role in atmospheric new particle formation (NPF). One of the major precursor species is α -pinene, which upon oxidation can form a suite of products covering a wide range of volatilities. Highly oxygenated organic molecules (HOMs) comprise a fraction of the oxidation products formed. While it is known that HOMs contribute to secondary organic aerosol (SOA) formation, including NPF, they have not been well studied in newly formed particles due to their very low mass concentrations. Here we present gas- and particle-phase chemical composition data from experimental studies of α -pinene oxidation, including in the presence of isoprene, at temperatures $(-50 \text{ and } -30 \,^{\circ}\text{C})$ and relative humidities $(20 \,\% \text{ and } 60 \,\%)$ relevant in the upper free troposphere. The measurements took place at the CERN Cosmics Leaving Outdoor Droplets (CLOUD) chamber. The particle chemical composition was analyzed by a thermal desorption differential mobility analyzer (TD-DMA) coupled to a nitrate chemical ionizationatmospheric pressure interface-time-of-flight (CI-APi-TOF) mass spectrometer. CI-APi-TOF was used for particle- and gas-phase measurements, applying the same ionization and detection scheme. Our measurements revealed the presence of C_{8-10} monomers and C_{18-20} dimers as the major compounds in the particles (diameter up to $\sim 100 \, \mathrm{nm}$). Particularly, for the system with isoprene added, C₅ (C₅H₁₀O₅₋₇) and C₁₅ compounds (C₁₅H₂₄O₅₋₁₀) were detected. This observation is consistent with the previously observed formation of such compounds in the gas phase. However, although the C₅ and C₁₅ compounds do not easily nucleate, our measurements indicate that they can still contribute to the particle growth at free tropospheric conditions. For the experiments reported here, most likely isoprene oxidation products enhance the growth of particles larger than 15 nm. Additionally, we report on the nucleation rates measured at 1.7 nm $(J_{1.7 \text{ nm}})$ and compared with previous studies, we found lower $J_{1.7\,\mathrm{nm}}$ values, very likely due to the higher α -pinene and ozone mixing ratios used in the present study.

1 Introduction

Approximately half of the global cloud condensation nuclei (CCN) are produced by nucleation (Merikanto et al., 2009; Gordon et al., 2017). In particular, biogenic emissions of volatile organic compounds (VOCs) play an important role in the formation of aerosol particles. The chemical reactions involving VOCs can lead to the formation of highly oxygenated organic molecules (HOMs), which can be described as a class of organic compounds that are formed under atmospherically relevant conditions by gas-phase autoxidation involving peroxy radicals (Ehn et al., 2014; Bianchi et al., 2019). These compounds possess low-saturation vapor pressures and are thus relevant for secondary organic aerosol (SOA) formation, including new particle formation (NPF), due to gas-to-particle partitioning.

Isoprene (C₅H₈) has the highest global emission rate, and many studies have demonstrated the importance of isoprene in terms of SOA formation (Surratt et al., 2006, 2007, 2010; Paulot et al., 2009; Lin et al., 2012; Riva et al., 2016). α -Pinene $(C_{10}H_{16})$, while less abundant, is one of the most commonly observed and prominent contributors to biogenic SOA due to its ability to form HOMs that nucleate on their own under atmospheric conditions (Kirkby et al., 2016; Tröstl et al., 2016). The formation of SOA has been well studied in isoprene and α -pinene systems. The role of HOMs in SOA formation and NPF has also been explored in α pinene and α -pinene with isoprene systems. However, much less is known about the particle-phase composition of HOMs in these systems and the specific controls particle formation and growth rates, including as a function of temperature and the ratio of isoprene to α -pinene.

Regarding α -pinene studies, Stolzenburg et al. (2018) reported α -pinene dark ozonolysis experiments at +25, +5, and -25 °C and showed that the rapid growth of organic particles is observed across these temperatures and that higher T leads to a faster autoxidation, while lower T leads to an increased partitioning due to decreased vapor pressures. Furthermore, Simon et al. (2020) extended the study of α -pinene gaseous oxidation products to even lower temperatures from +25 to -50 °C, showing that the oxygen-to-carbon ratio (O:C) and the yield for HOM formation decrease as the temperature decreases, whereas the reduction of volatility com-

²⁵Aerosol and Haze Laboratory, Beijing Advanced Innovation Center for Soft Matter Science and Engineering, Beijing University of Chemical Technology, Beijing, 100029, China

²⁶Moscow Institute of Physics and Technology, National Research University, 117303, Moscow, Russia

pensates for this effect by increasing the nucleation rates at lower temperatures.

Kiendler-Scharr et al. (2009) presented observations at $15\,^{\circ}\text{C}$ of a significant decrease in particle number and volume concentration by the presence of isoprene in an experiment under plant-emitted VOC conditions. Subsequently, McFiggans et al. (2019) showed that isoprene, carbon monoxide, and methane can each suppress aerosol mass and the yield from monoterpenes in mixtures of atmospheric vapors. Recently, a study by Heinritzi et al. (2020) revealed that the presence of isoprene in the α -pinene system suppresses new particle formation by altering the peroxy-radical termination reactions and inhibiting the formation of those molecules needed for the first steps of cluster and particle formation (species with 19 to 20 carbon atoms).

Despite the difficulties in measuring the nanoparticle chemical composition due to their very small mass, there have been several efforts for designing and improving techniques to face this problem. Some particle-phase studies exist that report the chemical composition of newly formed nanoparticles. For instance, Kristensen et al. (2017), measuring at -15 and +20 °C, showed an increased contribution of less oxygenated species to α -pinene SOA particles formed from ozonolysis at sub-zero temperatures. Ye et al. (2019) measured the particle-phase chemical composition from α -pinene oxidation between -50 and +25 °C with the FIGAERO inlet (Lopez-Hilfiker et al., 2014). They found that during new particle formation from α -pinene oxidation, gas-phase chemistry directly determines the composition of the condensed phase. Highly oxygenated organic molecules are much more abundant in particles formed at higher temperatures, shifting the compounds towards higher O: C and lower volatilities. Additionally, some studies addressing the chemical composition, volatility, and viscosity of organic molecules have provided important insights into their influence on the climate (Huang et al., 2018; Reid et al., 2018; Champion et al., 2019).

Here, we present the results from gas- and particle-phase chemical composition measurements for a system where α -pinene was oxidized to simulate pure biogenic new particle formation at free tropospheric conditions in a range from -50 to $-30\,^{\circ}$ C. The data are further compared to the mixed system of α -pinene and isoprene in order to better understand the partitioning processes. The particle chemical composition was analyzed by a thermal desorption differential mobility analyzer (TD-DMA) (Wagner et al., 2018), coupled to a nitrate chemical ionization–atmospheric pressure interface–time-of-flight (CI-APi-TOF) mass spectrometer. This technique allows for a direct comparison between the gas and particle phase as both measurements are using the identical chemical ionization source and detector.

2 Methods

2.1 The CLOUD chamber at CERN and the experiments

The measurements took place in the Cosmics Leaving Outdoor Droplets (CLOUD) chamber at the European Organization for Nuclear Research (CERN) during the CLOUD14 campaign (September-November 2019). The CLOUD chamber is a stainless-steel cylinder, with a volume of 26.1 m³, which has been built to the highest technical standards of cleanliness (Kirkby et al., 2011; Duplissy et al., 2016). By precisely controlling several parameters, such as gas concentrations, temperature, relative humidity, ultraviolet light intensity, and internal mixing, specific atmospheric systems can be recreated in order to study the nucleation and growth processes of aerosols at atmospheric conditions. The biogenic gas concentrations, here α -pinene and isoprene, can be regulated by using individual evaporator supplies, in which dry nitrogen passes through the evaporator containing the precursors in a liquid form, at controlled temperature. In this way, the precursors are evaporated and diluted with clean air to achieve the desired concentration in the chamber. Ozone is introduced via a separate gas line. The chamber is continuously stirred by two magnetically coupled stainlesssteel fans placed at the top and at the bottom of the chamber to provide a homogeneously mixed system (Voigtländer et al., 2012). In order to promote particle production from ions, galactic cosmic ray (GCR) conditions can be achieved by turning off the high voltage field $(30 \,\mathrm{kV} \,\mathrm{m}^{-1})$. The equilibrium ion-pair concentration in the chamber due to GCR is around $700 \,\mathrm{cm}^{-3}$ (Kirkby et al., 2016).

The experiments relevant for this work were done under GCR conditions and in a flow-through mode with continuous addition of the reactants, performed at -50 and $-30\,^{\circ}$ C, at low and high relative humidity to simulate pure biogenic new particle formation at a range of free tropospheric conditions. Isoprene and α -pinene precursor gases were oxidized with O_3 and \cdot OH (produced from O_3 photolysis in the presence of H_2O and UV light) to induce both dark ozonolysis and photochemistry oxidation reactions. The α -pinene level was between 1 and 8 ppby, the isoprene level up to 30 ppby, and O_3 approximately 100 ppby. The ozonolysis of α -pinene was performed at -50 and $-30\,^{\circ}$ C, while the α -pinene + isoprene experiment was performed at $-30\,^{\circ}$ C only. The experimental overview is discussed in more detail in Sect. 3.1.

2.2 TD-DMA

The particle chemical composition was analyzed by a thermal desorption differential mobility analyzer (TD-DMA) coupled to a nitrate chemical ionization—atmospheric pressure interface—time-of-flight (CI-APi-TOF) mass spectrometer. The TD-DMA design and characterization have been

described in detail by Wagner et al. (2018). This instrument allows for the direct comparison between gas- and particle-phase chemical composition as both measurements use the same ionization scheme and mass spectrometer (the detection technique will be described in Sect. 2.3).

The TD-DMA uses an online and semi-continuous principle for the detection of the chemical composition of nanoparticles. The particles are sampled from the chamber and charged with an X-ray source; a specific size can be selected, and immediately afterwards they are electrostatically collected on a filament. Heating the filament after a defined collection time evaporates the particles into a stream of clean carrier gas (N₂). The particle vapor is analyzed by the nitrate CI-APi-TOF mass spectrometer (Kürten et al., 2014). In order to estimate the instrumental background, two heating profiles are recorded: the first heating cycle evaporates all the particulate material collected; a second heating cycle constrains the background due to the heating of the inlet line. All reported particle-phase signals are corrected based on this background measurement.

For the experiments that are reported in this work, a filament of platinum/rhodium (90:10) was used, and an integral, non-size-selective mode of operation was chosen in order to maximize the mass of collected particles. For desorbing the sample, an electric current was applied to the filament and ramped linearly over a duration of approximately 1 min. Due to the very low experimental temperatures, cold sheath flows and isolated inlet lines were installed in order to avoid drastic temperature changes between the CLOUD chamber and the instrument. Evaporation of particulate material before the active heating should therefore not be substantial.

2.3 Nitrate CI-APi-TOF mass spectrometer

The gas-phase and the evaporated particulate material were measured using a nitrate chemical ionization-atmospheric pressure interface-time-of-flight (CI-APi-TOF) mass spectrometer, which has three major components: an atmospheric pressure ion-molecule reactor, where the chemical ionization takes place; an atmospheric pressure interface for transporting the charged ions into the mass classifier; and a time-offlight mass classifier, where the ions are accelerated, separated according to their mass-to-charge ratio, and detected with a microchannel plate (Jokinen et al., 2012; Kürten et al., 2014). The nitrate CI-APi-TOF mass spectrometer uses nitrate reagent ions $(HNO_3)_n NO_3^-$ with n = 0-2, which are created by an ion source using a corona discharge needle (Kürten et al., 2011). With this nitrate chemical ionization technique, sulfuric acid, iodic acid, dimethylamine and HOMs can be detected (Kürten et al., 2014; Simon et al., 2016; Kirkby et al., 2016; He et al., 2021). HOMs are detected because of the presence of functional groups such as hydroperoxy (-OOH) or hydroxy (-OH), which provide the hydrogen bonds required for clustering with the reagent ions. Here the nitrate CI-APi-TOF mass spectrometer data for the gas and particle phase have been corrected for background signals and the mass-dependent transmission efficiency in the mass classifier (Heinritzi et al., 2016). The data analysis and processing were performed using IGOR Pro 7 (WaveMetrics, Inc., USA), Tofware (Version 3.2, Aerodyne Inc., USA) and MATLAB R2019b (MathWorks, Inc., USA).

2.4 Nucleation rates

The particle number size distribution between ~ 1 nm and 1 µm is measured using a suite of particle counters namely a particle size magnifier (PSM; Vanhanen et al., 2011), a condensational particle counter (CPC 3776, TSI), a nano scanning mobility particle sizer (nano-SMPS 3982, TSI), and a home-built long scanning mobility particle sizer (long-SMPS). The PSM measures the size distribution between ~ 1 and 3 nm as well as the total particle number concentration above a defined cutoff, 1.7 nm in this study. The CPC on the other hand is used to measure the total particle number concentration above 2.5 nm. The nano-SMPS and long-SMPS together cover the particle number size distribution between 6 nm and 1 µm. The same setup has been used in previous CLOUD experiments; see for example Lehtipalo et al. (2018) and Heinritzi et al. (2020).

The nucleation rate (J_{dp}) , which is defined as the flux of particles of a certain size, is calculated using the method proposed by Dada et al. (2020); see Eq. (9) therein. For this study, the formation of particles with a diameter ≥ 1.7 nm is calculated $(J_{1.7})$ using the derivative of the total concentration of particles measured with the PSM while accounting for size-dependent losses to the chamber wall, by coagulation or via dilution. The error on $J_{1.7}$ is 30 % based on run-to-run repeatability (Dada et al., 2020).

3 Results and discussion

3.1 Experimental overview

An overview of the experiments performed at -30 and $-50\,^{\circ}\mathrm{C}$ at low and high relative humidity is shown in Fig. 1. The mixing ratio of ozone was stable at $\sim 100\,\mathrm{ppbv}$ for all of the experiments reported in this work (not shown). In order to represent pure biogenic new particle formation events, no other trace gases were added to the chamber, and the levels of SO_2 , NO_x , and other trace gases were monitored to remain always below the detection limits of the respective measurement devices. By using the TD-DMA, particles were collected in every NPF system (without resolving the particle size); the shaded area in Fig. 1 refers to the period where the particle collection took place.

The upper panel of Fig. 1 displays the size distribution measured by the scanning mobility particle sizer (SMPS). Four different experiments can be categorized as follows:

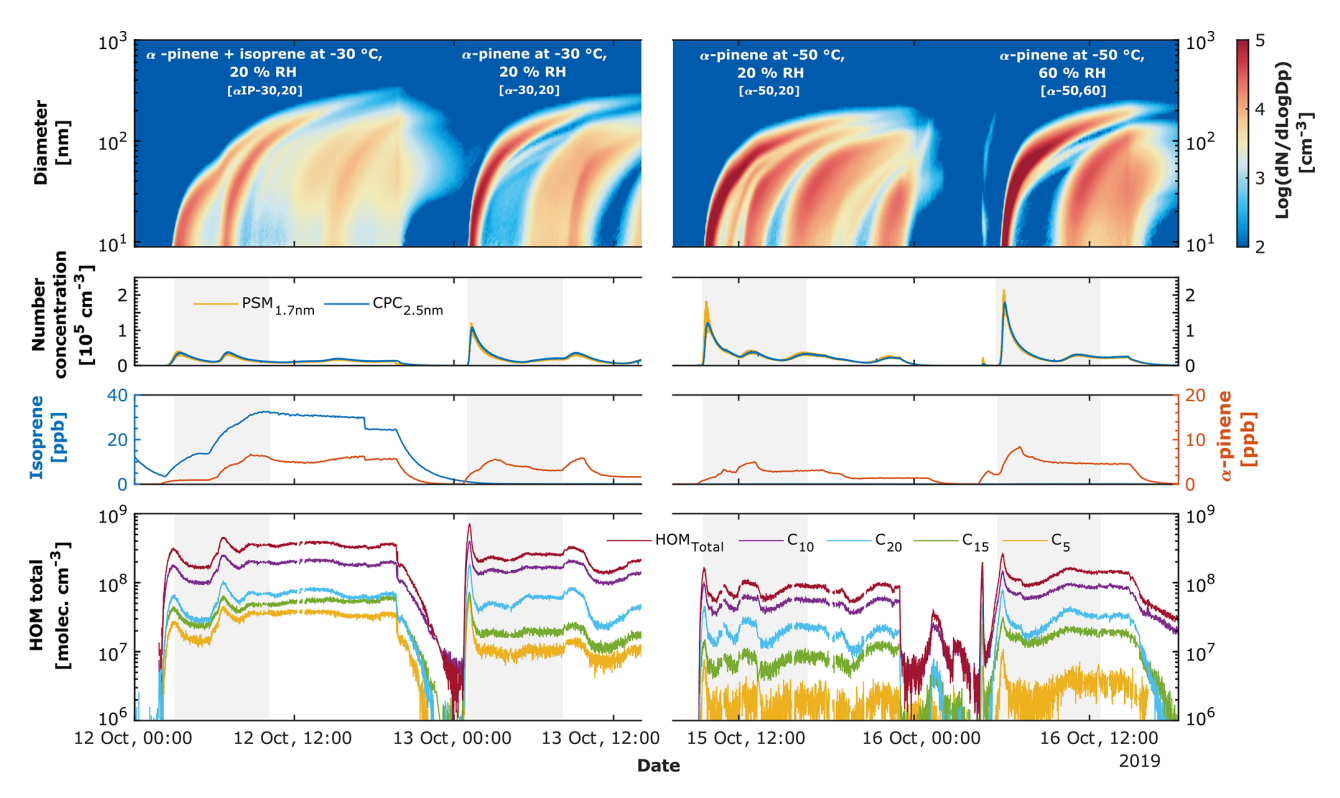


Figure 1. Experimental overview for pure biogenic new particle formation. First panel: particle size distribution for four different experiments: α -pinene + isoprene at -30 °C and 20 % RH (α IP-30,20), α -pinene at -30 °C and 20 % RH (α -30,20), α -pinene at -50 °C and 20 % RH (α -50,20), and α -pinene at -50 °C and 60 % RH (α -50,60). The color scale represents the log 10 of the normalized particle concentration in cubic centimeters (cm⁻³). Second panel: particle number concentration in cm⁻³ measured by the PSM with a cutoff diameter of 1.7 nm and CPC 2.5 nm. Third panel: mixing ratio in parts per billion by volume (ppbv) for the biogenic precursor gases, isoprene, and α -pinene. Fourth panel: evolution of total HOM concentration in molecules per cubic centimeter (molec. cm⁻³), measured in the gas phase by the nitrate CI-APi-TOF mass spectrometer. The HOM total is defined as the sum of C₅, C₁₀, C₁₅, and C₂₀ carbon classes, which are shown as well. Ozone level is not shown though remains stable over the whole period at \sim 100 ppbv. The shaded areas refer to the time when the particles were collected using the TD-DMA.

- 1. α -pinene + isoprene at -30 °C and 20 % RH (αIP -30,20),
- 2. α -pinene at -30 °C and 20 % RH (α -30,20),
- 3. α -pinene at -50 °C and 20 % RH (α -50,20), and
- 4. α -pinene at -50 °C and 60 % RH (α -50,60).

The color scale in the upper panel of Fig. 1 indicates that the newly formed particles appear in the smallest size channels of the SMPS soon after the concentration of α -pinene in the chamber is increased. The experiments were performed such that the particles grew rapidly to reach sizes of approximately 100 nm, where they could potentially act as cloud condensation nuclei (CCN) or ice nucleating particles (INPs) and were used for further CCN and INP studies.

The second panel of Fig. 1 shows the particle number concentration measured by the condensation particle counter (CPC_{2.5 nm}) and by the particle size magnifier (PSM) with a cutoff diameter of 1.7 nm. A higher particle number concentration can be observed for the experiments α -50,20 and

 α -50,60 at -50 °C, reaching $\sim 2 \times 10^5$ cm⁻³. By comparing the experiments at -30 °C, α -30,20, and α IP-30,20 a lower particle concentration is observed for the system where isoprene is present. The reduction is approximately a factor of 3; this can be attributed to the suppression of the new particle formation by isoprene oxidation. This is in line with the results of Kiendler-Scharr et al. (2009), who first reported the decrease in particle number of the nucleated particles. The effect of isoprene in terms of total HOM concentration in the gas phase and on the measured nucleation rates will be discussed in more detail in Sect. 3.4.2.

The third panel of Fig. 1 shows the α -pinene and isoprene mixing ratios. For all of the systems, α -pinene was between 1 and 8 ppbv, while isoprene was only present during experiment αIP -30,20 up to 30 ppbv. The precursor gases were measured by using a proton transfer reaction time-of-flight (PTR-TOF) mass spectrometer (Graus et al., 2010; Breitenlechner et al., 2017), which is capable of measuring VOCs.

The bottom panel of Fig. 1 shows the total HOM concentration in the gas phase. Here, the total HOM concentra-

tion is defined as the sum of C_5 , C_{10} , C_{15} , and C_{20} carbon classes; these classes consider compounds with C_2 – C_5 , C_6 – C_{10} , C_{11} – C_{15} , and C_{16} – C_{20} , respectively, and considered as a HOM such compounds with five or more oxygen atoms, as suggested in Bianchi et al. (2019). The total HOM concentration was measured with a calibrated nitrate CI-APi-TOF mass spectrometer (Kürten et al., 2012). Additionally, a temperature-dependent sampling loss correction factor is applied. From the evolution of these traces, it can be observed that C_5 and C_{15} carbon classes have higher concentrations (approximately by a factor of 2.5) in experiment α IP-30,20 compared with α -30,20, which can be explained by the presence of isoprene. However, possible fragmentation in the α -pinene ozonolysis systems also can lead to some C_5 and C_{15} compounds produced without the presence of isoprene.

3.2 Gas- and particle-phase chemical composition

Figure 2 shows the carbon distribution as an overview of the compounds detected in gas and particle phase for a system where only α -pinene was oxidized (α -30,20). C_{8-10} monomers (Fig. 2a) and C_{18-20} (Fig. 2b) dimers are observed in the gas as well as in the particle phase. For instance, some of the signals with the highest intensity correspond to $C_{10}H_{16}O_{3-9}$ and $C_{20}H_{32}O_{5-13}$; in particular $C_{10}H_{16}O_6$ and $C_{10}H_{16}O_7$ have an important presence in both phases. Overall, most of the compounds that are present in the gas phase are detected as well in the particle phase, although their relative contribution to the total signal can differ between the phases. The corresponding carbon distribution for the other systems can be found in Figs. S1 and S2 in the Supplement.

3.2.1 Influence of isoprene on α-pinene system at -30 °C and 20 % RH

Figure 3 shows mass defect plots of gas and particle phase and the intensity difference between each phase at $-30\,^{\circ}$ C. Figure 3a and d display the gas and particle composition of α -30,20, while the gas and particle composition of α IP-30,20 are shown in Fig. 3b and e, respectively. As both phases were measured with the same instrument, they can be directly inter-compared.

The intensity difference is calculated based on the normalized signal (each single signal divided by the total signal for each system and phase). Essentially, the normalized signal can be understood as a measure of the fraction or contribution of every compound in the entire system. By looking at the intensity difference in the gas phase (Fig. 3c), it can be observed that some C_5 and C_{15} contribute significantly more in the system with isoprene added (αIP -30,20) that are not as pronounced in the system where only α -pinene was oxidized (α -30,20). This observation can be attributed to the presence of isoprene in the system. As described by Heinritzi et al. (2020), C_{15} dimers are formed in the gas phase when C_{10} RO $_2^{\bullet}$ radicals from α -pinene ozonolysis undergo

terminating reactions with C_5 RO₂ radicals from the isoprene oxidation with ·OH. Additionally, C_{19} and C_{20} dimers contribute more in the system where only α -pinene was oxidized (α -30,20).

Figure 3f shows the intensity difference in the particle phase. In contrast with what is observed in the gas phase, the particle-phase effects seem more diverse. There is an increase in the intensity difference for several species in the system with isoprene (αIP -30,20), such as C₄₋₅, C₁₃₋₁₆, and some C_{17-19} (see Fig. S1 in the Supplement). In particular, a distinct group of C₁₅ compounds C₁₅H₂₄O₅₋₁₀ and $C_5H_{10}O_{5-7}$ can be identified in the particle and in the gas phase. A previous study has shown that isoprene can enhance particle growth rates despite its negative effect on nucleation (Heinritzi et al., 2020). The identification of C₁₅ dimers in nanometer-sized particles in the present study confirms this with a direct measurement. The suppressing effect of isoprene on nucleation will further be discussed in Sect. 3.4.2. However, isoprene can still contribute to the growth of particles by C_5 or by C_{15} compounds. Additionally, these species can be an important fingerprint to identify SOA formation from a mixture of biogenic vapors containing isoprene.

For the experiments presented in this study, we report in Table 1 the particle growth rates (GRs) determined from the nano-scanning electrical mobility spectrometer (nSEMS) size distributions. The growth rates in 3.2-8 and 5-15 nm were calculated using the 50 % appearance time method described in Stolzenburg et al. (2018). From the calculated values in Table 1, we observe that $GR_{3.2-8\,\mathrm{nm}}$ for the α pinene + isoprene system (αIP -30,20) at the first concentration stage is around 18 nm h^{-1} compared to $\sim 77 \text{ nm h}^{-1}$ for the α -pinene only system (α -30,20). This is a factor of \sim 4 difference, while GR_{5-15 nm} represents a factor of 2 to 3 difference between αIP -30,20 compared to α -30,20. From these values, one would conclude that isoprene does not contribute to the growth in the size range reported here. Nevertheless, by looking at the aerosol mass concentration (see Fig. S3 in the Supplement), the mass reached during the experiment αIP -30,20 is identical in the presence and absence of isoprene at -30 °C and 20 % RH. Reaching the same mass with a lower number of particles for the experiment with isoprene (αIP -30,20) compared to α -30,20 means that the growth rates at larger sizes (> 15 nm) are higher in the presence of isoprene. This is consistent with the fact that the particle size reached in the presence of isoprene is higher. Most likely, isoprene might enhance growth at larger sizes (> 15 nm) in the present study.

3.2.2 Influence of relative humidity on α -pinene system at -50 °C

Figure 4 shows mass defect plots for the pure α -pinene experiments at $-50\,^{\circ}$ C at low and high relative humidity: the gas and particle phase of α -pinene at $-50\,^{\circ}$ C, 20 % RH (Fig. 4a and d), and the gas and particle phase of α -pinene at $-50\,^{\circ}$ C,

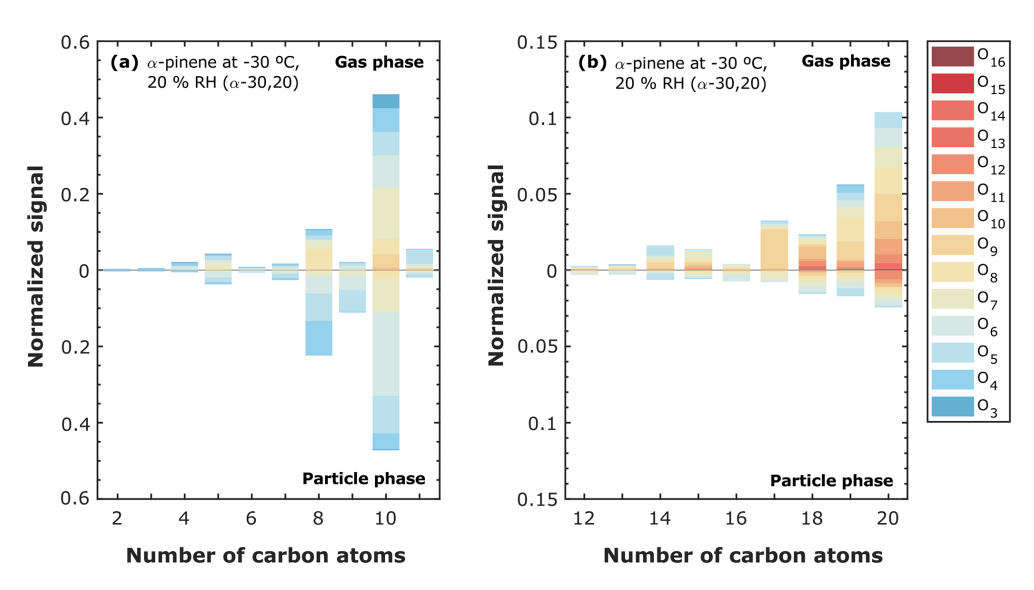


Figure 2. Carbon atom distribution and oxygen atom content in gas- and particle-phase molecules for α -pinene oxidation products at $-30\,^{\circ}$ C and $20\,\%$ RH (α -30,20). Both phases are measured with a nitrate CI-APi-TOF mass spectrometer, while the TD-DMA is coupled to it for particle-phase measurements. (a) Carbon atom distribution C_{2-11} and (b) carbon atom distribution C_{12-20} . The level of α -pinene was between 1 and 8 ppbv, and the ozone level was stable at \sim 100 ppbv. The intensities are normalized by the total signal in each system and phase. Each color represents a specific number of oxygen atoms in the range of 3 to 16.

Table 1. Summary of the main parameters for four pure biogenic new particle formation experiments.

| Experiment | Isoprene [ppb] | α-pinene [ppb] | Isoprene-to- monoterpene carbon ratio (R) | Ozone [ppb] | T [°C] | RH [%] | HOM total ^a [molec. cm ⁻³] | $[\text{cm}^{-3} \text{s}^{-1}]^{7}$ | Growth rate 3.2–8 nm [nm h ⁻¹] | Growth rate 5–15 nm [nm h ⁻¹] | $\begin{array}{c} \text{Mass}_{<15\text{nm}}/\\ \text{Mass}_{>15\text{nm}}^{b}\\ \text{[\%]} \end{array}$ |
|------------|-------------------|-------------------|---|-----------------|------------|-----------|---|---------------------------------------|--|---|---|
| αIP-30,20 | 13.71 31.38 | 0.95 5.12 | 14.4 6.1 | 98.58 101.56 | -30 -30 | 20 20 | 1.50e8 3.04e8 | 7.29 10.10 | 18.0 n/a | 22.8 39.0 | 0.29/99.7 |
| α-30,20 | ~0 | 3.35 | n/a | 102.10 | -30 | 20 | 2.20e8 | 23.76 | 76.9 | 77.1 | 0.11/99.9 |
| α-50,20 | ~0 | 3.04 | n/a | 100.55 | -50 | 20 | 6.72e7 | 51.24 | 41.1 | 42.0 | 0.26/99.7 |
| α-50,60 | ~0 | 7.72 | n/a | 110.20 | -50 | 60 | 8.00e7 | 79.17 | 63.4 | 78.4 | 0.09/99.9 |

^a Run-to-run experimental uncertainties of HOMs is \pm 20 %, and for $J_{1.7}$ it is \pm 30 %. n/a: not applicable. ^b Mass fraction of particles collected on the filament during the TD-DMA collection time, the calculation of which is based on SMPS mass distributions.

60 % RH (Fig. 4b and e). In both gas and particle phase at high and low RH, we detected C_{8-10} monomers and C_{18-20} dimers. $C_{10}H_{16}O_{4-7}$ and $C_{20}H_{32}O_{5-11}$ are the most prominent signals (see Fig. S2 in the Supplement).

The relative humidity change from 20% to 60% does not have a significant influence on the gas-phase composition at temperatures of $-50\,^{\circ}\mathrm{C}$ (Fig. 4c), meaning that most of the gaseous compounds detected contribute practically equal to the total signal when the humidity changes over the reported range. In contrast, there are changes in the particle-phase signal. The intensity difference (Fig. 4f) does not show a clear humidity effect on the particle chemical composition; however, this comparison is based on the normalized signal (contribution of every compound to the total intensity). When looking only at the total intensity in the particle phase, we do observe an increase by a factor of ~ 3 in the total signal for the system at high RH (α -50,60) compared with the system at

low RH (α -50,20). This observation can likely be attributed to a change in the particle mass size distribution (see Fig. S3 in the Supplement), which indicates that at similar α -pinene and ozone mixing ratio, and the same temperature, the particle mass concentration increases possibly due to the effect of the relative humidity in the system. In addition, a possible impact of relative humidity on particle viscosity can influence particle mass formed; studies by Grayson et al. (2016) and Galeazzo et al. (2021) have reported lower viscosity with higher SOA mass concentration along with RH dependence of viscosity for organic particles.

Our findings are consistent with previous experiments. Saathoff et al. (2009) observed that humidity has a significant influence on α -pinene SOA yields for lower temperatures. Cocker III et al. (2001) reported that the yield of SOA at higher RH for α -pinene ozonolysis (relative to the system at dry conditions) increases possibly due to the uptake

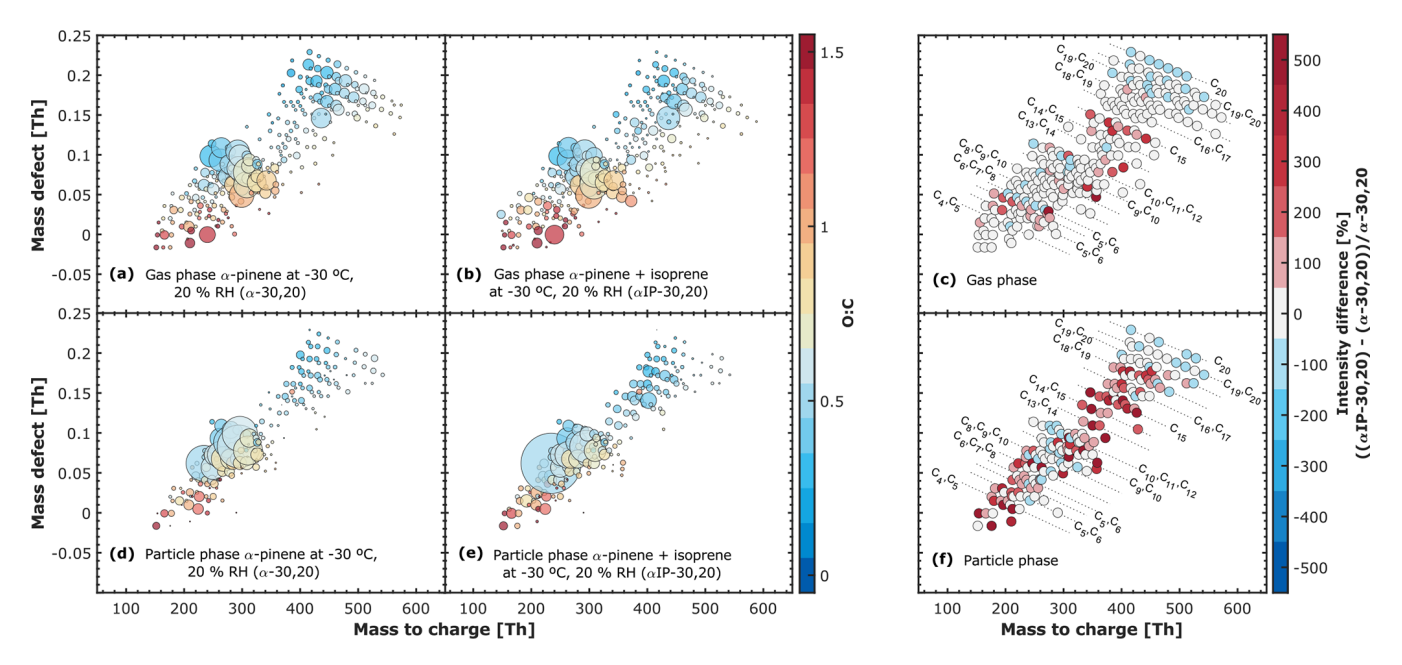


Figure 3. Mass defect plots of gas and particle phase and the intensity difference between each phase. Both phases are measured with a nitrate CI-APi-TOF mass spectrometer, while the TD-DMA is coupled to it for particle-phase measurements. (a) Gas and (d) particle phase for α-pinene oxidation products at -30 °C and 20 % RH (α-30,20). (b) Gas and (e) particle phase for α-pinene + isoprene oxidation products at -30 °C and 20 % RH (αIP-30,20). The level of α-pinene was between 1 and 8 ppbv in both experiments, while isoprene was present only in experiment αIP-30,20 reaching up to 30 ppbv. Ozone levels were ~ 100 ppbv in both experiments. The symbol sizes in (a), (b), (d), and (e) are the intensities normalized by the total signal in each system. The intensity difference in the gas phase (c) and in the particle phase (f) is indicated as $((\alpha IP-30,20) - (\alpha-30,20)) / (\alpha-30,20)$. The color scale represents the difference in percent.

of water. One explanation for this observation could be that the rate constant value of the α -pinene ozonolysis can be affected by the RH (Zhang et al., 2018). Nevertheless, our semi-continuous particle-phase measurements do not allow any conclusions on the magnitude of the rate constants to be drawn. Continuous particle-phase measurements under different RH conditions are required in order to better understand the RH effect on the SOA formation.

In general, for the experiments presented in this work, most of the compounds that are present in the gas phase are detected as well in the particle phase, although the relative contributions to the total signal can vary depending on the phase. The more oxygenated material in the gas phase, specifically for C_{20} dimers with $n_O > 13$, is not observed in the particle phase. This is probably because of their very low concentrations and the difficulty to distinguish between real particle signal and background. We conjecture that especially at low temperatures this issue might be related to the fact that at lower temperatures, the autoxidation process to form HOMs is slower; therefore, the oxygen content and O: C decrease (Stolzenburg et al., 2018; Ye et al., 2019; Simon et al., 2020). The low contribution of these compounds in the gas phase might be reflected in the particle phase. Additionally, the heating cycle that evaporates all the particulate material collected on the filament can potentially result in the thermal decomposition of some of the larger molecular-weight compounds. Therefore, it is possible that a break-up of some molecules occurs.

3.3 Volatility distribution of particle-phase compounds

Figure 5 shows the volatility distribution of the oxidation products in the particle phase measured by the TD-DMA for the experiments reported in this work (in linear scale Fig. S4 in the Supplement). The volatility calculation was done by using the parametrization introduced by Donahue et al. (2011) and modified by Stolzenburg et al. (2018) and Simon et al. (2020). It is expressed as the logarithm of the saturation mass concentration, $\log_{10}c_i^*$, in micrograms per cubic meters (µg m⁻³), from the number of carbon and oxygen atoms in the specific molecules. This approximation parameterizes the volatility of a molecule based on its functional groups and a free parameter to distinguish between monomers and dimers.

In Fig. 5 each volatility bin contains the summed intensity of the oxidation products measured in the particle phase, and it is normalized by the total signal. Most of the classes are distributed over the range of the volatility values that are displayed, and at lower temperatures, lower volatilities are observed (experiments α -50,20 and α -50,60). This observation is due to the fact of the strong dependency between saturation concentration and temperature. Essentially, there are no significant differences between the experiments at $-30\,^{\circ}\mathrm{C}$

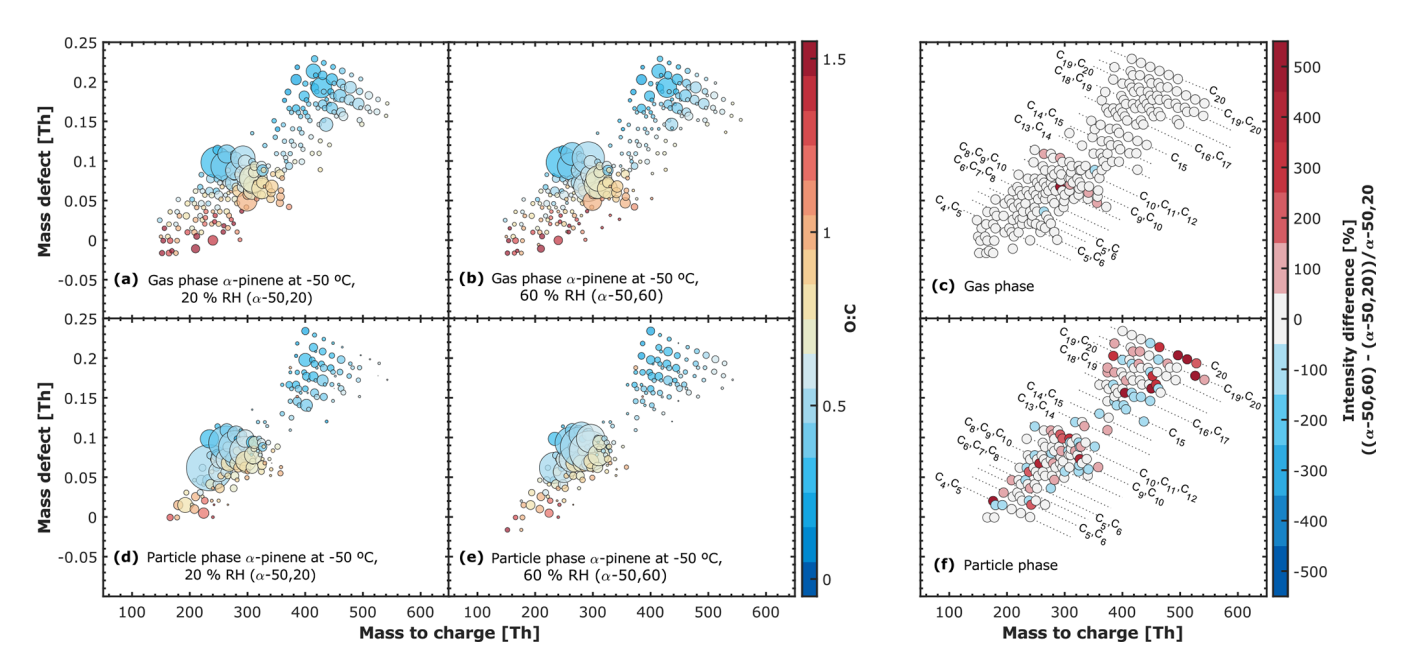


Figure 4. Mass defect plots of gas and particle phase and the intensity difference between each phase. Both phases are measured with a nitrate CI-APi-TOF mass spectrometer, while the TD-DMA is coupled to it for particle-phase measurements. (a) Gas and (d) particle phase for α-pinene oxidation products at -50 °C and 20 % RH (α-50,20). (b) Gas and (e) particle phase for α-pinene oxidation products at -50 °C and 60 % RH (α-50,60). The level of α-pinene was between 1 and 8 ppbv, and ozone levels were \sim 100 ppbv in both experiments. The symbol sizes in (a), (b), (d), and (e) are the intensities normalized by the total signal in each system. The intensity difference in the gas phase (c) and in the particle phase (f) is indicated as $((\alpha-50,60)-(\alpha-50,20))/(\alpha-50,20)$. The color scale represents the difference in percent.

 $(\alpha-30,20)$ compared with α *IP-30,20*) or between the experiments at -50 °C (α -50,20 compared with α -50,60), which indicates that temperature is the main parameter affecting the volatility distribution for the experiments reported here.

We classified the volatility bins according to the regimes proposed by Donahue et al. (2012) and Schervish and Donahue (2020) and calculated the corresponding fractions (Table 2). Overall, the particle-phase-detected compounds correspond mainly to low-volatility organic compounds (LVOCs) and extremely low-volatility compounds (ELVOCs) by explaining more than 80% of the signals, while ultralow-volatility organic compounds (ULVOCs) represent only a small fraction (between 6% and 17%). With this parametrization, we are able to approximate the saturation mass concentration for the particle-phase compounds measured using the TD-DMA in the CLOUD chamber. For this parametrization, we assume that the elemental composition is one of the main parameters to take into account.

3.4 Nucleation rates as a function of the total HOM concentration

Previous CLOUD studies have reported nucleation rates $(J_{1.7\,\mathrm{nm}})$ as a function of the total HOM concentration from α -pinene oxidation for different temperatures and gas mixtures (Kirkby et al., 2016; Heinritzi et al., 2020; Simon et al., 2020). For the experiments discussed in the present study, the nucleation rates have not been reported yet. For this rea-

son, Table 1 gives an overview of the experimental conditions for the experiments α -30,20, α IP-30,20, α -50,20, and α -50,60; it further includes the HOM total concentration and derived $J_{1.7\,\mathrm{nm}}$ from the PSM data (see method description in Sect. 2.4).

3.4.1 New particle formation on pure α -pinene experiments

Figure 6 displays pure biogenic $J_{1.7 \text{ nm}}$ vs total HOM concentration at different temperatures for pure α -pinene (Simon et al., 2020) in which it can be seen that the total HOM concentration and their nucleation rates have a strong dependence on the temperature. As the temperature decreases, the nucleation rates increase strongly for a given HOM concentration. In other terms, the total HOM concentration needed to reach the same nucleation rate can be up to 2 orders of magnitude higher for +25 °C compared to -50 °C. As described by Simon et al. (2020), this can be attributed to the reduction in volatility with decreasing temperature. In other words, at low temperatures, molecules with less oxygen content can lead to the same nucleation rate as more highly oxygenated molecules at higher temperatures. Additionally, Fig. 6 includes the data points at -30 and -50 °C from pure α -pinene experiments reported in this study (α -30,20, α -50,20 and α -50,60). However, it can be observed that they do not follow the trend at their corresponding temperature.

| Table 2. | Bin | volatility | fractions | for the | different | experiments. |
|----------|-----|------------|-----------|---------|-----------|--------------|
| | | | | | | |

| Experiment | T | RH | ULVOCs | ELVOCs | LVOCs | SVOCs | IVOCs |
|--|-----------------------|----------------------------|----------------------------|------------------------------|------------------------------|--------------------------|---------------|
| | [°C] | [%] | [%] | [%] | [%] | [%] | [%] |
| αIP-30,20 α-30,20 α-50,20 α-50,60 | -30 -30 -50 -50 | 20 20 20 20 60 | 8.6 5.9 16.5 13.8 | 28.3 44.1 36.4 50.6 | 59.1 48.1 46.1 34.8 | 3.8 1.9 1.0 0.8 | 0.2 0 0 |

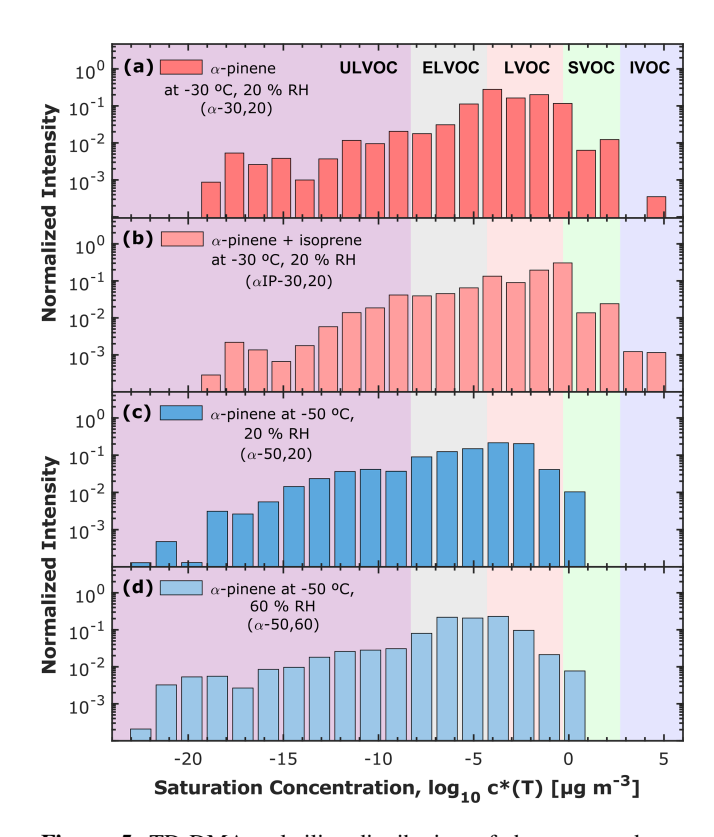


Figure 5. TD-DMA volatility distribution of the measured oxidation products in the particle phase for four different experiments: (a) α -pinene at $-30\,^{\circ}$ C and $20\,^{\circ}$ RH (α -30,20), (b) α -pinene + isoprene at $-30\,^{\circ}$ C and $20\,^{\circ}$ RH (α IP-30,20), (c) α -pinene at $-50\,^{\circ}$ C and $20\,^{\circ}$ RH (α -50,20), and (d) α -pinene at $-50\,^{\circ}$ C and $60\,^{\circ}$ RH (α -50,60). Every individual volatility bin includes the sum of the intensity for the oxidation products normalized by the total signal in each system. Every individual volatility bin is defined at 300 K, shifted, and widened according to their corresponding temperature. The color bands in the background indicate the volatility regimes as in Donahue et al. (2012) and in Schervish and Donahue (2020). The normalized intensity is dimensionless. Nevertheless, it should be noted that the particle-phase signal is given in normalized counts per second integrated over the evaporation time (ncps/s).

For the pure α -pinene systems (α -30,20, α -50,20, and α -50,60) and complementary pure α -pinene experiments at +5 °C and at -10 °C, we have calculated the HOM yield as described in Simon et al. (2020) and found that the result-

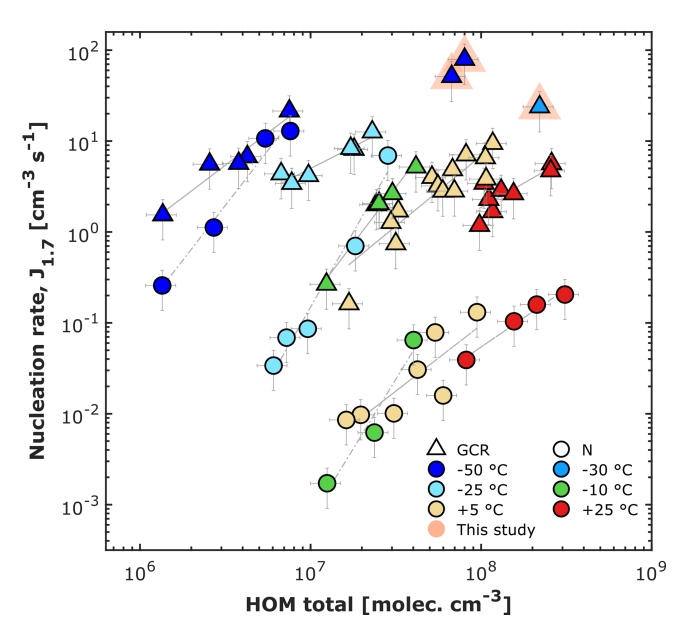


Figure 6. Pure biogenic nucleation rates of pure α -pinene at 1.7 nm diameter against total HOM concentration at different temperatures. The HOM total is defined as the sum of C_5 , C_{10} , C_{15} and C_{20} carbon classes. Triangles represent galactic cosmic ray (GCR) conditions, and circles represent neutral conditions. Data points at -50, -25, -10, +5, and $+25\,^{\circ}\mathrm{C}$ are from Simon et al. (2020). The points with orange marker on the background are the contribution of this study (experiments α -30,20, α -50,20 and α -50,60). Solid and dashed lines represent power-law fits to GCR and neutral conditions. Bars indicate 1σ run-to-run experimental uncertainty. The overall systematic-scale uncertainty of HOMs of $+78\,\%$ and $-68\,\%$ is not shown.

ing values are higher than previously reported (see Fig. S5 in the Supplement). In order to investigate a possible reason for this finding, we have chosen two representative experiments at $-10\,^{\circ}$ C and $80\,\%$ RH to $90\,\%$ RH with different levels of α -pinene and ozone. Figure 7 shows the mass defect plots for the gas-phase chemical composition of the oxidation products. In one experiment (Fig. 7a) α -pinene and the ozone mixing ratio were between 0.2 and 0.8 ppbv and 40 and 50 ppbv, respectively, while for the second experiment (Fig. 7b) the mixing ratios were 2 to 3 ppbv and 100 ppbv, respectively. From Fig. 7c, it can be concluded that the formation of HOMs with low oxygen content is favored when

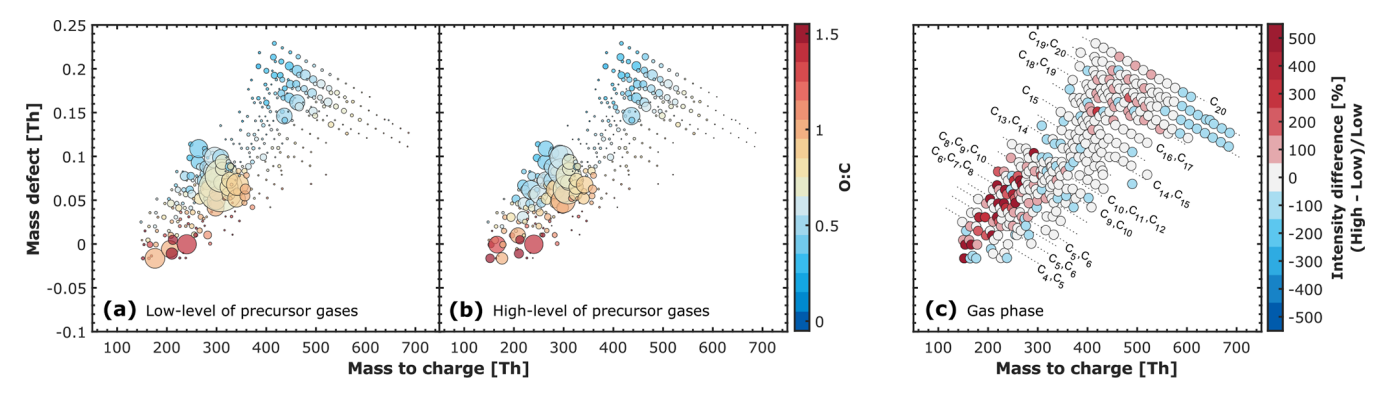


Figure 7. Mass defect plots of gas phase for two different systems and the normalized difference between them. Gas phase is measured with a nitrate CI-APi-TOF mass spectrometer. (a) α -Pinene oxidation products at $-10\,^{\circ}$ C and 90 % RH at low level of precursor gases and (b) α -pinene oxidation products at $-10\,^{\circ}$ C and 80 % RH at high level of precursor gases. α -pinene was 0.2–0.8 ppbv and ozone \sim 40–50 ppbv in (a), and α -pinene was 2–3 ppbv and ozone \sim 100 ppbv in (b). The symbol sizes and colors in (a) and (b) represent the intensities normalized by the total signal in each system. (c) The difference between the normalized signals shown in (a) and (b) is represented by the color scale.

the α -pinene and ozone mixing ratio are higher (relative to the system at low levels of precursor gases). An explanation for this is that the high concentration of RO2 enhances the terminating reactions before the autoxidation can lead to high oxygen content for the products. As the compounds with low oxygen content tend to have higher saturation vapor pressures, they do not contribute efficiently to new particle formation. For this reason, a given total HOM concentration is not unambiguously tied to a nucleation rate (even at constant temperature). The magnitude of the precursor gas mixing ratio (more specifically the full volatility distribution of the products and not just the simple measure of total HOM concentration) also needs to be taken into account (see Fig. S6 in the Supplement). In summary, the lower $J_{1.7 \, \text{nm}}$ values compared with previous studies are very likely due to the higher α -pinene and ozone mixing ratios used in the present study. There are several compounds with low oxygen content that contribute to the total HOM concentration in the gas phase, while these do not contribute to the formation of new particles.

3.4.2 The influence of isoprene on new particle formation

In order to make the present study comparable with other studies that reported a suppression effect of isoprene on biogenic new particle formation, the values of the isoprene-to-monoterpene carbon ratio (R) are also provided in Table 1. Here and in previous studies, R is essentially the ratio between isoprene and α -pinene; for experiment αIP -30,20, R is equal to 14.4 and 6.1 (for two steady-state periods in αIP -30,20).

Figure 8 shows pure biogenic nucleation rates at 1.7 nm against total HOM concentration at different temperatures for the α -pinene and α -pinene + isoprene systems (Kirkby

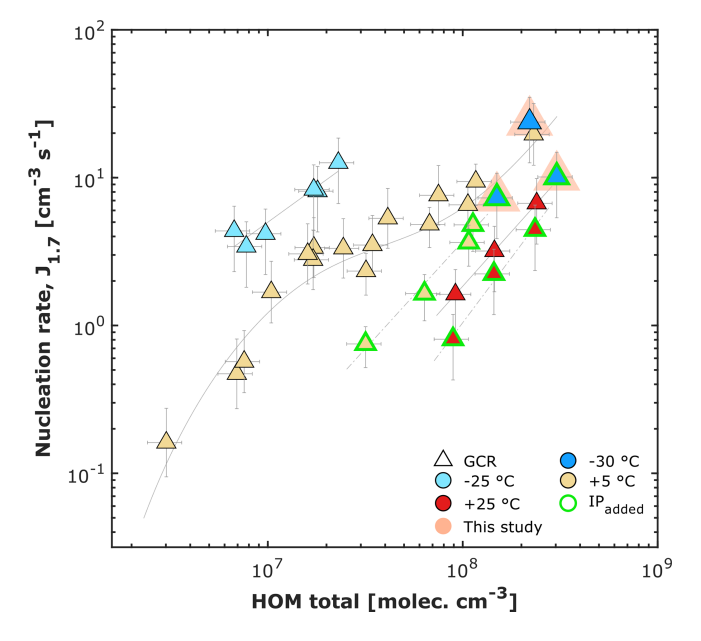


Figure 8. Pure biogenic nucleation rates at 1.7 nm diameter against total HOM concentration at different temperatures for α -pinene and α -pinene + isoprene systems. The HOM total is defined as the sum of C₅, C₁₀, C₁₅, and C₂₀ carbon classes. Triangles represent galactic cosmic ray (GCR) conditions. Data points at +5 and +25 °C are from Kirkby et al. (2016) and Heinritzi et al. (2020). Data points at -25 °C are from Simon et al. (2020). The value of isoprene-tomonoterpene carbon ratio (*R*) varies from 1.5 to 6.5 for Heinritzi et al. (2020), and *R* is equal to 14.4 and 6.1 for this study. The points with orange marker on the background indicate the contribution of this work. Solid lines represent power-law fits to GCR conditions of the systems with α -pinene only, and dashed lines are the power-law fits of the systems with isoprene added. Bars indicate 1 σ run-to-run experimental uncertainty. The overall systematic-scale uncertainty of HOMs of +78 % and -68 % is not shown.

et al., 2016; Heinritzi et al., 2020; Simon et al., 2020). How rapidly particles are formed in a pure biogenic system depends strongly on the temperature and on the ion conditions. In general, we observe increasing nucleation rates at lower temperatures and at GCR conditions. The presence of isoprene lowers the nucleation rate (relative to the pure α pinene system at similar conditions); this is known as isoprene suppression of new particle formation. In this regard, there is a suppression on the new particle formation caused by adding isoprene on an α -pinene system at -30 °C and 20 % RH. However, it has been reported that the suppression effect is stronger when α -pinene is lower (and R is higher; see Fig. S7 in the Supplement). For instance, in a plant chamber experiment R = 19.5 resulted in no significant new particle formation (Kiendler-Scharr et al., 2009). Additionally, in the Michigan forest with R = 26.4, NPF events did not occur frequently (Kanawade et al., 2011). Lee et al. (2016) reported observations of NPF suppression in a rural forest in Alabama, where R = 2.0. However, one has to consider that the suppression effect at a given value of R likely decreases as temperature decreases and so does the saturation vapor pressure of the oxidation products.

4 Conclusions

In this study, we demonstrated the suitability of a thermal desorption differential mobility analyzer (TD-DMA) coupled to a nitrate chemical ionization—atmospheric pressure interface—time-of-flight (CI-APi-TOF) mass spectrometer for measuring HOMs in newly formed nano aerosol particles. Together with the nitrate CI-APi-TOF mass spectrometer, this setup is capable of measuring the gas and particle phase, allowing for a direct comparison as both measurements use the identical chemical ionization and detector.

For the pure biogenic NPF experiments performed at -50 and $-30\,^{\circ}\text{C}$ in the CLOUD chamber at CERN, we detected in the particle phase (diameter up to $\sim 100\,\text{nm}$) compounds such as $C_{10}H_{16}O_{3-9}$, and $C_{20}H_{32}O_{5-13}$. Especially for the system with isoprene added, C_5 ($C_5H_{10}O_{5-7}$) and C_{15} compounds ($C_{15}H_{24}O_{5-10}$) can be an important fingerprint to identify secondary organic aerosol from this biogenic source. Based on the elemental composition, we calculated the saturation mass concentration, and according to the volatility regimes, the particle-phase compounds correspond mainly to low-volatility organic compounds (LVOCs), extremely low-volatility compounds (ELVOCs), and ultralow-volatility organic compounds (ULVOCs).

We also showed that at $-30\,^{\circ}\mathrm{C}$ and an isoprene-to-monoterpene carbon ratio R=14.4 and 6.1, there is a reduction of the nucleation rate (compared to the pure α -pinene system at similar conditions). In this way, isoprene suppresses NPF at $-30\,^{\circ}\mathrm{C}$. Nevertheless, this suppression effect can be stronger at higher temperatures and at high R.

Lastly, the lower $J_{1.7}$ values compared with previous studies are very likely due to the higher α -pinene and ozone mixing ratios used in the present study. There are several compounds with low oxygen content that contribute to the total HOM concentration in the gas phase, while these do not contribute to the formation of new particles. For this reason, a given total HOM concentration is not unambiguously tied to a nucleation rate (even at constant temperature). The magnitude of the precursor gas mixing ratio, and thus the full volatility distribution, also needs to be taken into account.

Data availability. Data related to this article are available upon request to the corresponding authors.

Supplement. The supplement related to this article is available online at: https://doi.org/10.5194/acp-21-17099-2021-supplement.

Author contributions. LC, BR, GM, MaS, ACW, TM, MG, FA, RB, BB, ZB, RC, BC, JD, HF, LGC, XCH, VH, WK, HL, CPL, BL, NGAM, VM, HEM, RM, RLM, BM, UM, AO, JP, MP, AAP, WS, BS, JS, DS, YS, MiS, YJT, PT, AT, SV, MW, DSW, SKW, AW, WY, WY, MZW, UB, IEH, RCF, KH, JK, MK, KL, OM, RV, PMW, AK, and JC prepared the CLOUD facility and measurement instruments. LC, BR, GM, ACW, TM, MG, AA, FA, RB, BB, JD, LGC, VH, HL, CPL, NGAM, VM, RM, DM, RLM, BM, UM, WS, BS, DS, MiS, CT, YJT, AT, DSW, SKW, MZW, IEH, JK, RV, and PMW collected the data. LC, BR, MH, GM, FA, LD, RLM, UM, WS, BS, SKW, and RCF analyzed the data. LC, MH, MSim, ACW, TM, MG, LD, RLM, UM, MiS, WS, DS, UB, IEH, RCF, AH, KH, JK, MK, OM, HS, NMD, AK, and JC contributed to the scientific discussion and interpretation of the results. LC, MH, ACW, LD, UB, RCF, HS, NMD, AK, and JC contributed to the writing of the manuscript.

Competing interests. The contact author has declared that neither they nor their co-authors have any competing interests.

Disclaimer. Publisher's note: Copernicus Publications remains neutral with regard to jurisdictional claims in published maps and institutional affiliations.

Acknowledgements. We thank CERN for providing the CLOUD facility to perform the experiments and the CLOUD community for supporting this study. We especially would like to thank Katja Ivanova, Timo Keber, Frank Malkemper, Robert Sitals, Hanna Elina Manninen, Antti Onnela, and Robert Kristic for their contributions to the experiment.

Financial support. This research has been supported by the European Commission, Research Executive Agency (grant no. CLOUD-MOTION (764991)), the Bundesministerium für Bildung

und Forschung (grant no. CLOUD-16, 01LK1601A), the National Science Foundation (grant nos. AGS-1801280, AGS-1801574, and AGS-1801897), and the Schweizerischer Nationalfonds zur Förderung der Wissenschaftlichen Forschung (grant nos. 20020_172602 and BSSGI0_155846).

This open-access publication was funded by the Goethe University Frankfurt.

Review statement. This paper was edited by Kelley Barsanti and reviewed by two anonymous referees.

References

- Bianchi, F., Kurtein, T., Riva, M., Mohr, C., Rissanen, M. P., Roldin, P., Berndt, T., Crounse, J. D., Wennberg, P. O., and Mentel, T. F.: Highly oxygenated organic molecules (HOM) from gas-phase autoxidation involving peroxy radicals: A key contributor to atmospheric aerosol, Chem. Rev., 119, 3472–3509, 2019.
- Breitenlechner, M., Fischer, L., Hainer, M., Heinritzi, M., Curtius, J., and Hansel, A.: PTR3: An Instrument for Studying the Lifecycle of Reactive Organic Carbon in the Atmosphere, Anal. Chem., 89, 5824–5831, 10.1021/acs.analchem.6b05110, 2017.
- Champion, W. M., Rothfuss, N. E., Petters, M. D., and Grieshop, A. P.: Volatility and Viscosity Are Correlated in Terpene Secondary Organic Aerosol Formed in a Flow Reactor, Environ. Sci. Technol. Lett., 6, 513–519, https://doi.org/10.1021/acs.estlett.9b00412, 2019.
- Cocker III, D. R., Clegg, S. L., Flagan, R. C., and Seinfeld, J. H.: The effect of water on gas–particle partitioning of secondary organic aerosol, Part I: α-pinene/ozone system, Atmos. Environ., 35, 6049–6072, https://doi.org/10.1016/j.jes.2017.10.011, 2001.
- Dada, L., Lehtipalo, K., Kontkanen, J., Nieminen, T., Baalbaki, R., Ahonen, L., Duplissy, J., Yan, C., Chu, B., Petäjä, T., Lehtinen, K., Kerminen, V.-M., Kulmala, M., and Kangasluoma, J.: Formation and growth of sub-3-nm aerosol particles in experimental chambers, Nat. Protoc., 15, 1013–1040, https://doi.org/10.1038/s41596-019-0274-z, 2020.
- Donahue, N. M., Epstein, S. A., Pandis, S. N., and Robinson, A. L.: A two-dimensional volatility basis set: 1. organic-aerosol mixing thermodynamics, Atmos. Chem. Phys., 11, 3303–3318, https://doi.org/10.5194/acp-11-3303-2011, 2011.
- Donahue, N. M., Kroll, J. H., Pandis, S. N., and Robinson, A. L.: A two-dimensional volatility basis set Part 2: Diagnostics of organic-aerosol evolution, Atmos. Chem. Phys., 12, 615–634, https://doi.org/10.5194/acp-12-615-2012, 2012.
- Duplissy, J., Merikanto, J., Franchin, A., Tsagkogeorgas, G., Kangasluoma, J., Wimmer, D., Vuollekoski, H., Schobesberger, S., Lehtipalo, K., Flagan, R. C., Brus, D., Donahue, N. M., Vehkamäki, H., Almeida, J., Amorim, A., Barmet, P., Bianchi, F., Breitenlechner, M., Dunne, E. M., Guida, R., Henschel, H., Junninen, H., Kirkby, J., Kürten, A., Kupc, A., Määttänen, A., Makhmutov, V., Mathot, S., Nieminen, T., Onnela, A., Praplan, A. P., Riccobono, F., Rondo, L., Steiner, G., Tome, A., Walther, H., Baltensperger, U., Carslaw, K. S., Dommen, J., Hansel, A., Petäjä, T., Sipilä, M., Stratmann, F., Vrtala, A., Wagner, P. E., Worsnop, D. R., Curtius, J., and Kulmala, M.: Ef-

- fect of ions on sulfuric acid-water binary particle formation: 2. Experimental data and comparison with QC-normalized classical nucleation theory, J. Geophys. Res.-Atmos., 121, 1752–1775, https://doi.org/10.1002/2015JD023539, 2016.
- Ehn, M., Thornton, J. A., Kleist, E., Sipila, M., Junninen, H., Pullinen, I., Springer, M., Rubach, F., Tillmann, R., Lee, B., Lopez-Hilfiker, F., Andres, S., Acir, I.-H., Rissanen, M., Jokinen, T., Schobesberger, S., Kangasluoma, J., Kontkanen, J., Nieminen, T., Kurten, T., Nielsen, L. B., Jorgensen, S., Kjaergaard, H. G., Canagaratna, M., Maso, M. D., Berndt, T., Petaja, T., Wahner, A., Kerminen, V.-M., Kulmala, M., Worsnop, D. R., Wildt, J., and Mentel, T. F.: A large source of low-volatility secondary organic aerosol, Nature, 506, 476–479, https://doi.org/10.1038/nature13032, 2014.
- Galeazzo, T., Valorso, R., Li, Y., Camredon, M., Aumont, B., and Shiraiwa, M.: Estimation of secondary organic aerosol viscosity from explicit modeling of gas-phase oxidation of isoprene and α-pinene, Atmos. Chem. Phys., 21, 10199–10213, https://doi.org/10.5194/acp-21-10199-2021, 2021.
- Gordon, H., Kirkby, J., Baltensperger, U., Bianchi, F., Breitenlechner, M., Curtius, J., Dias, A., Dommen, J., Donahue, N. M., Dunne, E. M., Duplissy, J., Ehrhart, S., Flagan, R. C., Frege, C., Fuchs, C., Hansel, A., Hoyle, C. R., Kulmala, M., Kürten, A., Lehtipalo, K., Makhmutov, V., Molteni, U., Rissanen, M. P., Stozkhov, Y., Tröstl, J., Tsagkogeorgas, G., Wagner, R., Williamson, C., Wimmer, D., Winkler, P. M., Yan, C., and Carslaw, K. S.: Causes and importance of new particle formation in the present-day and preindustrial atmospheres, J. Geophys. Res.-Atmos., 122, 8739–8760, https://doi.org/10.1002/2017jd026844, 2017.
- Graus, M., Müller, M., and Hansel, A.: High resolution PTR-TOF: Quantification and formula confirmation of VOC in real time, J. Am. Soc. Mass Sp., 21, 1037–1044, https://doi.org/10.1016/j.jasms.2010.02.006, 2010.
- Grayson, J. W., Zhang, Y., Mutzel, A., Renbaum-Wolff, L., Böge, O., Kamal, S., Herrmann, H., Martin, S. T., and Bertram, A. K.: Effect of varying experimental conditions on the viscosity of α-pinene derived secondary organic material, Atmos. Chem. Phys., 16, 6027–6040, https://doi.org/10.5194/acp-16-6027-2016, 2016.
- He, X.-C., Tham, Y. J., Dada, L., Wang, M., Finkenzeller, H., Stolzenburg, D., Iyer, S., Simon, M., Kürten, A., Shen, J., Rörup, B., Rissanen, M., Schobesberger, S., Baalbaki, R., Wang, D. S., Koenig, T. K., Jokinen, T., Sarnela, N., Beck, L. J., Almeida, J., Amanatidis, S., Amorim, A., Ataei, F., Baccarini, A., Bertozzi, B., Bianchi, F., Brilke, S., Caudillo, L., Chen, D., Chiu, R., Chu, B., Dias, A., Ding, A., Dommen, J., Duplissy, J., El Haddad, I., Gonzalez Carracedo, L., Granzin, M., Hansel, A., Heinritzi, M., Hofbauer, V., Junninen, H., Kangasluoma, J., Kemppainen, D., Kim, C., Kong, W., Krechmer, J. E., Kvashin, A., Laitinen, T., Lamkaddam, H., Lee, C. P., Lehtipalo, K., Leiminger, M., Li, Z., Makhmutov, V., Manninen, H. E., Marie, G., Marten, R., Mathot, S., Mauldin, R. L., Mentler, B., Möhler, O., Müller, T., Nie, W., Onnela, A., Petäjä, T., Pfeifer, J., Philippov, M., Ranjithkumar, A., Saiz-Lopez, A., Salma, I., Scholz, W., Schuchmann, S., Schulze, B., Steiner, G., Stozhkov, Y., Tauber, C., Tomé, A., Thakur, R. C., Väisänen, O., Vazquez-Pufleau, M., Wagner, A. C., Wang, Y., Weber, S. K., Winkler, P. M., Wu, Y., Xiao, M., Yan, C., Ye, Q., Ylisirniö, A., Zauner-Wieczorek, M., Zha, Q.,

- Zhou, P., Flagan, R. C., Curtius, J., Baltensperger, U., Kulmala, M., Kerminen, V.-M., Kurtén, T., Donahue, N. M., Volkamer, R., Kirkby, J., Worsnop, D. R., and Sipilä, M.: Role of iodine oxoacids in atmospheric aerosol nucleation, Science, 371, 589–595, https://doi.org/10.1126/science.abe0298, 2021.
- Heinritzi, M., Simon, M., Steiner, G., Wagner, A. C., Kürten, A., Hansel, A., and Curtius, J.: Characterization of the massdependent transmission efficiency of a CIMS, Atmos. Meas. Tech., 9, 1449–1460, https://doi.org/10.5194/amt-9-1449-2016, 2016.
- Heinritzi, M., Dada, L., Simon, M., Stolzenburg, D., Wagner, A. C., Fischer, L., Ahonen, L. R., Amanatidis, S., Baalbaki, R., Baccarini, A., Bauer, P. S., Baumgartner, B., Bianchi, F., Brilke, S., Chen, D., Chiu, R., Dias, A., Dommen, J., Duplissy, J., Finkenzeller, H., Frege, C., Fuchs, C., Garmash, O., Gordon, H., Granzin, M., El Haddad, I., He, X., Helm, J., Hofbauer, V., Hoyle, C. R., Kangasluoma, J., Keber, T., Kim, C., Kürten, A., Lamkaddam, H., Laurila, T. M., Lampilahti, J., Lee, C. P., Lehtipalo, K., Leiminger, M., Mai, H., Makhmutov, V., Manninen, H. E., Marten, R., Mathot, S., Mauldin, R. L., Mentler, B., Molteni, U., Müller, T., Nie, W., Nieminen, T., Onnela, A., Partoll, E., Passananti, M., Petäjä, T., Pfeifer, J., Pospisilova, V., Quéléver, L. L. J., Rissanen, M. P., Rose, C., Schobesberger, S., Scholz, W., Scholze, K., Sipilä, M., Steiner, G., Stozhkov, Y., Tauber, C., Tham, Y. J., Vazquez-Pufleau, M., Virtanen, A., Vogel, A. L., Volkamer, R., Wagner, R., Wang, M., Weitz, L., Wimmer, D., Xiao, M., Yan, C., Ye, P., Zha, Q., Zhou, X., Amorim, A., Baltensperger, U., Hansel, A., Kulmala, M., Tomé, A., Winkler, P. M., Worsnop, D. R., Donahue, N. M., Kirkby, J., and Curtius, J.: Molecular understanding of the suppression of new-particle formation by isoprene, Atmos. Chem. Phys., 20, 11809-11821, https://doi.org/10.5194/acp-20-11809-2020, 2020.
- Huang, W., Saathoff, H., Pajunoja, A., Shen, X., Naumann, K. H., Wagner, R., Virtanen, A., Leisner, T., and Mohr, C.: α-Pinene secondary organic aerosol at low temperature: chemical composition and implications for particle viscosity, Atmos. Chem. Phys., 18, 2883–2898, https://doi.org/10.5194/acp-18-2883-2018, 2018.
- Jokinen, T., Sipilä, M., Junninen, H., Ehn, M., Lönn, G., Hakala, J., Petäjä, T., Mauldin Iii, R. L., Kulmala, M., and Worsnop, D. R.: Atmospheric sulphuric acid and neutral cluster measurements using CI-APi-TOF, Atmos. Chem. Phys., 12, 4117–4125, https://doi.org/10.5194/acp-12-4117-2012, 2012.
- Kanawade, V. P., Jobson, B. T., Guenther, A. B., Erupe, M. E., Pressley, S. N., Tripathi, S. N., and Lee, S. H.: Isoprene suppression of new particle formation in a mixed deciduous forest, Atmos. Chem. Phys., 11, 6013–6027, https://doi.org/10.5194/acp-11-6013-2011, 2011.
- Kiendler-Scharr, A., Wildt, J., Maso, M. D., Hohaus, T., Kleist, E., Mentel, T. F., Tillmann, R., Uerlings, R., Schurr, U., and Wahner, A.: New particle formation in forests inhibited by isoprene emissions, Nature, 461, 381–384, 2009.
- Kirkby, J., Curtius, J., Almeida, J., Dunne, E., Duplissy, J., Ehrhart, S., Franchin, A., Gagné, S., Ickes, L., Kürten, A., Kupc, A., Metzger, A., Riccobono, F., Rondo, L., Schobesberger, S., Tsagkogeorgas, G., Wimmer, D., Amorim, A., Bianchi, F., Breitenlechner, M., David, A., Dommen, J., Downard, A., Ehn, M., Flagan, R. C., Haider, S., Hansel, A., Hauser, D., Jud, W., Junninen, H., Kreissl, F., Kvashin, A., Laaksonen, A., Lehtipalo, K.,

- Lima, J., Lovejoy, E. R., Makhmutov, V., Mathot, S., Mikkilä, J., Minginette, P., Mogo, S., Nieminen, T., Onnela, A., Pereira, P., Petäjä, T., Schnitzhofer, R., Seinfeld, J. H., Sipilä, M., Stozhkov, Y., Stratmann, F., Tomé, A., Vanhanen, J., Viisanen, Y., Vrtala, A., Wagner, P. E., Walther, H., Weingartner, E., Wex, H., Winkler, P. M., Carslaw, K. S., Worsnop, D. R., Baltensperger, U., and Kulmala, M.: Role of sulphuric acid, ammonia and galactic cosmic rays in atmospheric aerosol nucleation, Nature, 476, 429–433, https://doi.org/10.1038/nature10343, 2011.
- Kirkby, J., Duplissy, J., Sengupta, K., Frege, C., Gordon, H., Williamson, C., Heinritzi, M., Simon, M., Yan, C., Almeida, J., Tröstl, J., Nieminen, T., Ortega, I. K., Wagner, R., Adamov, A., Amorim, A., Bernhammer, A.-K., Bianchi, F., Breitenlechner, M., Brilke, S., Chen, X., Craven, J., Dias, A., Ehrhart, S., Flagan, R. C., Franchin, A., Fuchs, C., Guida, R., Hakala, J., Hoyle, C. R., Jokinen, T., Junninen, H., Kangasluoma, J., Kim, J., Krapf, M., Kürten, A., Laaksonen, A., Lehtipalo, K., Makhmutov, V., Mathot, S., Molteni, U., Onnela, A., Peräkylä, O., Piel, F., Petäjä, T., Praplan, A. P., Pringle, K., Rap, A., Richards, N. A. D., Riipinen, I., Rissanen, M. P., Rondo, L., Sarnela, N., Schobesberger, S., Scott, C. E., Seinfeld, J. H., Sipilä, M., Steiner, G., Stozhkov, Y., Stratmann, F., Tomé, A., Virtanen, A., Vogel, A. L., Wagner, A. C., Wagner, P. E., Weingartner, E., Wimmer, D., Winkler, P. M., Ye, P., Zhang, X., Hansel, A., Dommen, J., Donahue, N. M., Worsnop, D. R., Baltensperger, U., Kulmala, M., Carslaw, K. S., and Curtius, J.: Ion-induced nucleation of pure biogenic particles, Nature, 533, 521-526, https://doi.org/10.1038/nature17953, 2016.
- Kristensen, K., Jensen, L., Glasius, M., and Bilde, M.: The effect of sub-zero temperature on the formation and composition of secondary organic aerosol from ozonolysis of alpha-pinene, Environ. Sci. Proc. Imp., 19, 1220–1234, 2017.
- Kürten, A., Rondo, L., Ehrhart, S., and Curtius, J.: Performance of a corona ion source for measurement of sulfuric acid by chemical ionization mass spectrometry, Atmos. Meas. Tech., 4, 437–443, https://doi.org/10.5194/amt-4-437-2011, 2011.
- Kürten, A., Rondo, L., Ehrhart, S., and Curtius, J.: Calibration of a Chemical Ionization Mass Spectrometer for the Measurement of Gaseous Sulfuric Acid, J. Phys. Chem. A, 116, 6375–6386, https://doi.org/10.1021/jp212123n, 2012.
- Kürten, A., Jokinen, T., Simon, M., Sipilä, M., Sarnela, N., Junninen, H., Adamov, A., Almeida, J., Amorim, A., Bianchi, F., Breitenlechner, M., Dommen, J., Donahue, N. M., Duplissy, J., Ehrhart, S., Flagan, R. C., Franchin, A., Hakala, J., Hansel, A., Heinritzi, M., Hutterli, M., Kangasluoma, J., Kirkby, J., Laaksonen, A., Lehtipalo, K., Leiminger, M., Makhmutov, V., Mathot, S., Onnela, A., Petäjä, T., Praplan, A. P., Riccobono, F., Rissanen, M. P., Rondo, L., Schobesberger, S., Seinfeld, J. H., Steiner, G., Tomé, A., Tröstl, J., Winkler, P. M., Williamson, C., Wimmer, D., Ye, P., Baltensperger, U., Carslaw, K. S., Kulmala, M., Worsnop, D. R., and Curtius, J.: Neutral molecular cluster formation of sulfuric acid–dimethylamine observed in real time under atmospheric conditions, P. Natl. Acad. Sci. USA, 111, 15019–15024, https://doi.org/10.1073/pnas.1404853111, 2014.
- Lee, S.-H., Uin, J., Guenther, A. B., de Gouw, J. A., Yu, F.,
 Nadykto, A. B., Herb, J., Ng, N. L., Koss, A., Brune, W.
 H., Baumann, K., Kanawade, V. P., Keutsch, F. N., Nenes,
 A., Olsen, K., Goldstein, A., and Ouyang, Q.: Isoprene suppression of new particle formation: Potential mechanisms and

- implications, J. Geophys. Res.-Atmos., 121, 14621–614635, https://doi.org/10.1002/2016JD024844, 2016.
- Lehtipalo, K., Yan, C., Dada, L., Bianchi, F., Xiao, M., Wagner, R., Stolzenburg, D., Ahonen, L. R., Amorim, A., Baccarini, A., Bauer, P. S., Baumgartner, B., Bergen, A., Bernhammer, A.-K., Breitenlechner, M., Brilke, S., Buchholz, A., Mazon, S. B., Chen, D., Chen, X., Dias, A., Dommen, J., Draper, D. C., Duplissy, J., Ehn, M., Finkenzeller, H., Fischer, L., Frege, C., Fuchs, C., Garmash, O., Gordon, H., Hakala, J., He, X., Heikkinen, L., Heinritzi, M., Helm, J. C., Hofbauer, V., Hoyle, C. R., Jokinen, T., Kangasluoma, J., Kerminen, V.-M., Kim, C., Kirkby, J., Kontkanen, J., Kürten, A., Lawler, M. J., Mai, H., Mathot, S., Mauldin, R. L., Molteni, U., Nichman, L., Nie, W., Nieminen, T., Ojdanic, A., Onnela, A., Passananti, M., Petäjä, T., Piel, F., Pospisilova, V., Quéléver, L. L. J., Rissanen, M. P., Rose, C., Sarnela, N., Schallhart, S., Schuchmann, S., Sengupta, K., Simon, M., Sipilä, M., Tauber, C., Tomé, A., Tröstl, J., Väisänen, O., Vogel, A. L., Volkamer, R., Wagner, A. C., Wang, M., Weitz, L., Wimmer, D., Ye, P., Ylisirniö, A., Zha, Q., Carslaw, K. S., Curtius, J., Donahue, N. M., Flagan, R. C., Hansel, A., Riipinen, I., Virtanen, A., Winkler, P. M., Baltensperger, U., Kulmala, M., and Worsnop, D. R.: Multicomponent new particle formation from sulfuric acid, ammonia, and biogenic vapors, Sci. Adv., 4, eaau5363, https://doi.org/10.1126/sciadv.aau5363, 2018.
- Lin, Y.-H., Zhang, Z., Docherty, K. S., Zhang, H., Budisulistiorini, S. H., Rubitschun, C. L., Shaw, S. L., Knipping, E. M., Edgerton, E. S., Kleindienst, T. E., Gold, A., and Surratt, J. D.: Isoprene Epoxydiols as Precursors to Secondary Organic Aerosol Formation: Acid-Catalyzed Reactive Uptake Studies with Authentic Compounds, Environ. Sci. Technol., 46, 250–258, https://doi.org/10.1021/es202554c, 2012.
- Lopez-Hilfiker, F. D., Mohr, C., Ehn, M., Rubach, F., Kleist, E., Wildt, J., Mentel, T. F., Lutz, A., Hallquist, M., Worsnop, D., and Thornton, J. A.: A novel method for online analysis of gas and particle composition: description and evaluation of a Filter Inlet for Gases and AEROsols (FIGAERO), Atmos. Meas. Tech., 7, 983–1001, https://doi.org/10.5194/amt-7-983-2014, 2014.
- McFiggans, G., Mentel, T. F., Wildt, J., Pullinen, I., Kang, S., Kleist, E., Schmitt, S., Springer, M., Tillmann, R., Wu, C., Zhao, D., Hallquist, M., Faxon, C., Le Breton, M., Hallquist, Å. M., Simpson, D., Bergström, R., Jenkin, M. E., Ehn, M., Thornton, J. A., Alfarra, M. R., Bannan, T. J., Percival, C. J., Priestley, M., Topping, D., and Kiendler-Scharr, A.: Secondary organic aerosol reduced by mixture of atmospheric vapours, Nature, 565, 587–593, https://doi.org/10.1038/s41586-018-0871-y, 2019.
- Merikanto, J., Spracklen, D. V., Mann, G. W., Pickering, S. J., and Carslaw, K. S.: Impact of nucleation on global CCN, Atmos. Chem. Phys., 9, 8601–8616, https://doi.org/10.5194/acp-9-8601-2009, 2009.
- Paulot, F., Crounse, J. D., Kjaergaard, H. G., Kürten, A., Clair, J. M. S., Seinfeld, J. H., and Wennberg, P. O.: Unexpected epoxide formation in the gas-phase photooxidation of isoprene, Science, 325, 730–733, 2009.
- Reid, J. P., Bertram, A. K., Topping, D. O., Laskin, A., Martin, S. T., Petters, M. D., Pope, F. D., and Rovelli, G.: The viscosity of atmospherically relevant organic particles, Nat. Commun., 9, 956, https://doi.org/10.1038/s41467-018-03027-z, 2018.
- Riva, M., Budisulistiorini, S. H., Zhang, Z., Gold, A., and Surratt, J. D.: Chemical characterization of secondary or-

- ganic aerosol constituents from isoprene ozonolysis in the presence of acidic aerosol, Atmos. Environ., 130, 5–13, https://doi.org/10.1016/j.atmosenv.2015.06.027, 2016.
- Saathoff, H., Naumann, K. H., Möhler, O., Jonsson, Å. M., Hallquist, M., Kiendler-Scharr, A., Mentel, T. F., Tillmann, R., and Schurath, U.: Temperature dependence of yields of secondary organic aerosols from the ozonolysis of α-pinene and limonene, Atmos. Chem. Phys., 9, 1551–1577, https://doi.org/10.5194/acp-9-1551-2009, 2009.
- Schervish, M. and Donahue, N. M.: Peroxy radical chemistry and the volatility basis set, Atmos. Chem. Phys., 20, 1183–1199, https://doi.org/10.5194/acp-20-1183-2020, 2020.
- Simon, M., Heinritzi, M., Herzog, S., Leiminger, M., Bianchi, F., Praplan, A., Dommen, J., Curtius, J., and Kürten, A.: Detection of dimethylamine in the low pptv range using nitrate chemical ionization atmospheric pressure interface time-of-flight (CI-APi-TOF) mass spectrometry, Atmos. Meas. Tech., 9, 2135–2145, https://doi.org/10.5194/amt-9-2135-2016, 2016.
- Simon, M., Dada, L., Heinritzi, M., Scholz, W., Stolzenburg, D., Fischer, L., Wagner, A. C., Kürten, A., Rörup, B., He, X. C., Almeida, J., Baalbaki, R., Baccarini, A., Bauer, P. S., Beck, L., Bergen, A., Bianchi, F., Bräkling, S., Brilke, S., Caudillo, L., Chen, D., Chu, B., Dias, A., Draper, D. C., Duplissy, J., El-Haddad, I., Finkenzeller, H., Frege, C., Gonzalez-Carracedo, L., Gordon, H., Granzin, M., Hakala, J., Hofbauer, V., Hoyle, C. R., Kim, C., Kong, W., Lamkaddam, H., Lee, C. P., Lehtipalo, K., Leiminger, M., Mai, H., Manninen, H. E., Marie, G., Marten, R., Mentler, B., Molteni, U., Nichman, L., Nie, W., Ojdanic, A., Onnela, A., Partoll, E., Petäjä, T., Pfeifer, J., Philippov, M., Ouéléver, L. L. J., Ranjithkumar, A., Rissanen, M. P., Schallhart, S., Schobesberger, S., Schuchmann, S., Shen, J., Sipilä, M., Steiner, G., Stozhkov, Y., Tauber, C., Tham, Y. J., Tomé, A. R., Vazquez-Pufleau, M., Vogel, A. L., Wagner, R., Wang, M., Wang, D. S., Wang, Y., Weber, S. K., Wu, Y., Xiao, M., Yan, C., Ye, P., Ye, Q., Zauner-Wieczorek, M., Zhou, X., Baltensperger, U., Dommen, J., Flagan, R. C., Hansel, A., Kulmala, M., Volkamer, R., Winkler, P. M., Worsnop, D. R., Donahue, N. M., Kirkby, J., and Curtius, J.: Molecular understanding of newparticle formation from α -pinene between -50 and +25 °C, Atmos. Chem. Phys., 20, 9183-9207, https://doi.org/10.5194/acp-20-9183-2020, 2020.
- Stolzenburg, D., Fischer, L., Vogel, A. L., Heinritzi, M., Schervish, M., Simon, M., Wagner, A. C., Dada, L., Ahonen, L. R., Amorim, A., Baccarini, A., Bauer, P. S., Baumgartner, B., Bergen, A., Bianchi, F., Breitenlechner, M., Brilke, S., Buenrostro Mazon, S., Chen, D., Dias, A., Draper, D. C., Duplissy, J., El Haddad, I., Finkenzeller, H., Frege, C., Fuchs, C., Garmash, O., Gordon, H., He, X., Helm, J., Hofbauer, V., Hoyle, C. R., Kim, C., Kirkby, J., Kontkanen, J., Kürten, A., Lampilahti, J., Lawler, M., Lehtipalo, K., Leiminger, M., Mai, H., Mathot, S., Mentler, B., Molteni, U., Nie, W., Nieminen, T., Nowak, J. B., Ojdanic, A., Onnela, A., Passananti, M., Petäjä, T., Quéléver, L. L. J., Rissanen, M. P., Sarnela, N., Schallhart, S., Tauber, C., Tomé, A., Wagner, R., Wang, M., Weitz, L., Wimmer, D., Xiao, M., Yan, C., Ye, P., Zha, Q., Baltensperger, U., Curtius, J., Dommen, J., Flagan, R. C., Kulmala, M., Smith, J. N., Worsnop, D. R., Hansel, A., Donahue, N. M., and Winkler, P. M.: Rapid growth of organic aerosol nanoparticles over a wide tropospheric

- temperature range, P. Natl. Acad. Sci. USA, 115, 9122–9127, https://doi.org/10.1073/pnas.1807604115, 2018.
- Surratt, J. D., Murphy, S. M., Kroll, J. H., Ng, N. L., Hildebrandt, L., Sorooshian, A., Szmigielski, R., Vermeylen, R., Maenhaut, W., Claeys, M., Flagan, R. C., and Seinfeld, J. H.: Chemical Composition of Secondary Organic Aerosol Formed from the Photooxidation of Isoprene, J. Phys. Chem. A, 110, 9665–9690, https://doi.org/10.1021/jp061734m, 2006.
- Surratt, J. D., Lewandowski, M., Offenberg, J. H., Jaoui, M., Kleindienst, T. E., Edney, E. O., and Seinfeld, J. H.: Effect of Acidity on Secondary Organic Aerosol Formation from Isoprene, Environ. Sci. Technol., 41, 5363–5369, https://doi.org/10.1021/es0704176, 2007.
- Surratt, J. D., Chan, A. W., Eddingsaas, N. C., Chan, M., Loza, C. L., Kwan, A. J., Hersey, S. P., Flagan, R. C., Wennberg, P. O., and Seinfeld, J. H.: Reactive intermediates revealed in secondary organic aerosol formation from isoprene, P. Natl. Acad. Sci. USA, 107, 6640–6645, 2010.
- Tröstl, J., Chuang, W. K., Gordon, H., Heinritzi, M., Yan, C., Molteni, U., Ahlm, L., Frege, C., Bianchi, F., Wagner, R., Simon, M., Lehtipalo, K., Williamson, C., Craven, J. S., Duplissy, J., Adamov, A., Almeida, J., Bernhammer, A.-K., Breitenlechner, M., Brilke, S., Dias, A., Ehrhart, S., Flagan, R. C., Franchin, A., Fuchs, C., Guida, R., Gysel, M., Hansel, A., Hoyle, C. R., Jokinen, T., Junninen, H., Kangasluoma, J., Keskinen, H., Kim, J., Krapf, M., Kürten, A., Laaksonen, A., Lawler, M., Leiminger, M., Mathot, S., Möhler, O., Nieminen, T., Onnela, A., Petäjä, T., Piel, F. M., Miettinen, P., Rissanen, M. P., Rondo, L., Sarnela, N., Schobesberger, S., Sengupta, K., Sipilä, M., Smith, J. N., Steiner, G., Tomè, A., Virtanen, A., Wagner, A. C., Weingartner, E., Wimmer, D., Winkler, P. M., Ye, P., Carslaw, K. S., Curtius, J., Dommen, J., Kirkby, J., Kulmala, M., Riipinen, I., Worsnop, D. R., Donahue, N. M., and Baltensperger, U.: The role of low-volatility organic compounds in initial particle growth in the atmosphere, Nature, 533, 527-531, https://doi.org/10.1038/nature18271, 2016.

- Vanhanen, J., Mikkilä, J., Lehtipalo, K., Sipilä, M., Manninen, H. E., Siivola, E., Petäjä, T., and Kulmala, M.: Particle Size Magnifier for Nano-CN Detection, Aerosol Sci. Technol., 45, 533–542, https://doi.org/10.1080/02786826.2010.547889, 2011.
- Voigtländer, J., Duplissy, J., Rondo, L., Kürten, A., and Stratmann, F.: Numerical simulations of mixing conditions and aerosol dynamics in the CERN CLOUD chamber, Atmos. Chem. Phys., 12, 2205–2214, https://doi.org/10.5194/acp-12-2205-2012, 2012.
- Wagner, A. C., Bergen, A., Brilke, S., Fuchs, C., Ernst, M., Hoker, J., Heinritzi, M., Simon, M., Bühner, B., Curtius, J., and Kürten, A.: Size-resolved online chemical analysis of nanoaerosol particles: a thermal desorption differential mobility analyzer coupled to a chemical ionization time-of-flight mass spectrometer, Atmos. Meas. Tech., 11, 5489–5506, https://doi.org/10.5194/amt-11-5489-2018, 2018.
- Ye, Q., Wang, M., Hofbauer, V., Stolzenburg, D., Chen, D., Schervish, M., Vogel, A. L., Mauldin, R. L., Baalbaki, R., Brilke, S., Dada, L., Dias, A., Duplissy, J., El Haddad, I., Finkenzeller, H., Fischer, L., He, X., Kim, C., Kürten, A., Lamkaddam, H., Lee, C. P., Lehtipalo, K., Leiminger, M., Manninen, H. E., Marten, R., Mentler, B., Partoll, E., Petäjä, T., Rissanen, M. P., Schobesberger, S., Schuchmann, S., Simon, M., Tham, Y. J., Vazquez-Pufleau, M., Wagner, A. C., Wang, Y., Wu, Y., Xiao, M., Baltensperger, U., Curtius, J., Flagan, R., Kirkby, j., Kulmala, M., Volkamer, R., Winkler, P. M., Worsnop, D. R., and Donahue, N. M.: Molecular Composition and Volatility of Nucleated Particles from α-Pinene Oxidation between -50°C and +25°C, Environ. Sci. Technol., 53, 12357–12365, https://doi.org/10.1021/acs.est.9b03265, 2019.
- Zhang, G., Fu, H., and Chen, J.: Effect of relative humidity and the presence of aerosol particles on the α -pinene ozonolysis, J. Environ. Sci., 71, 99–107, https://doi.org/10.1016/j.jes.2017.10.011, 2018.

Supplement of Atmos. Chem. Phys., 21, 17099–17114, 2021 https://doi.org/10.5194/acp-21-17099-2021-supplement © Author(s) 2021. CC BY 4.0 License.





Supplement of

Chemical composition of nanoparticles from α -pinene nucleation and the influence of isoprene and relative humidity at low temperature

Lucía Caudillo et al.

Correspondence to: Lucía Caudillo (lucia.caudillo@iau.uni-frankfurt.de) and Joachim Curtius (curtius@iau.uni-frankfurt.de)

The copyright of individual parts of the supplement might differ from the article licence.

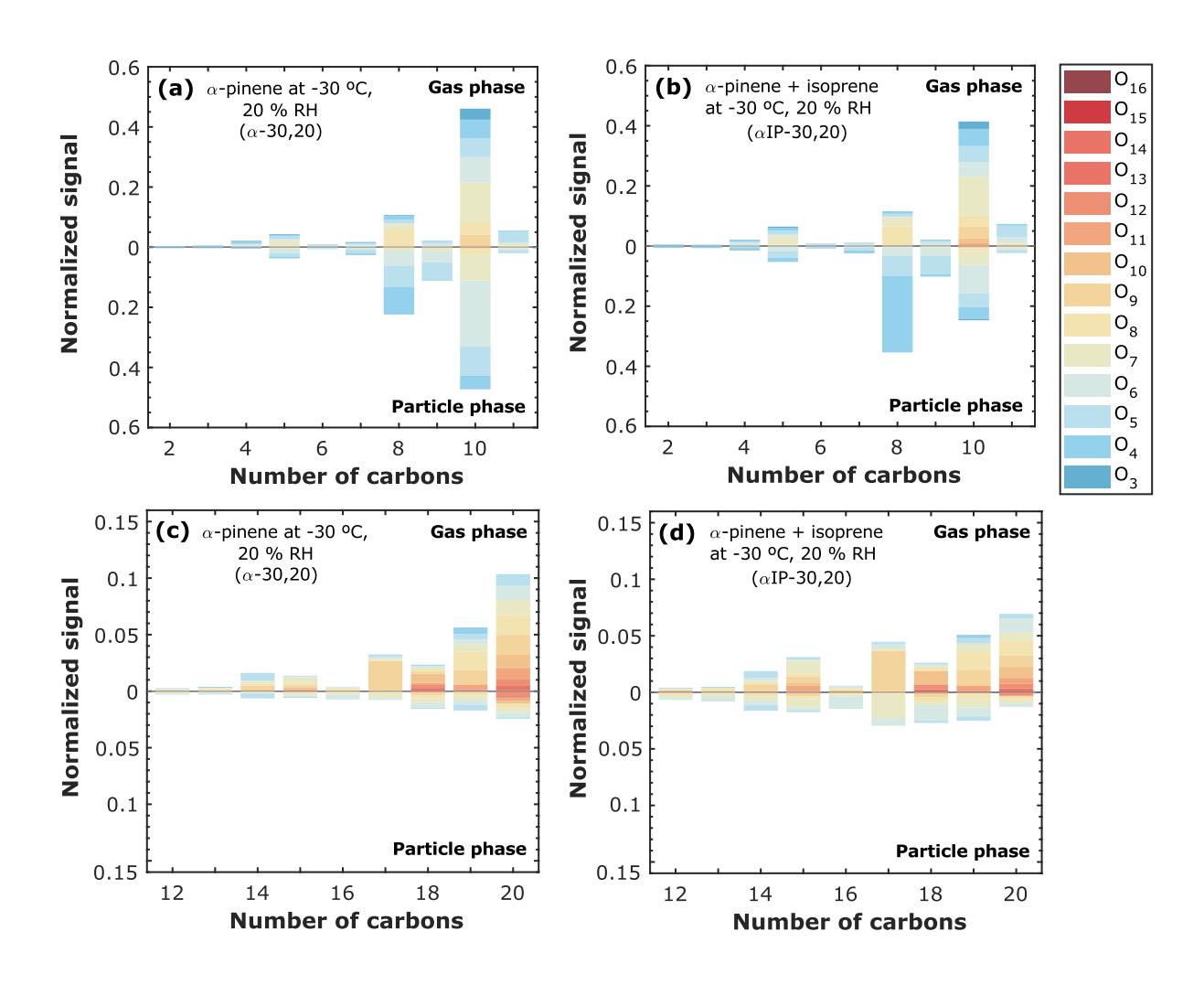


Figure S1. Carbon atom distribution C_{2-11} and C_{12-20} and oxygen atom content in gas and particle phase molecules. Both phases are measured with a Nitrate CI-APi-TOF mass spectrometer, while the TD-DMA is coupled to it for particle phase measurements. (a) and (c) α -pinene oxidation products at -30 °C and 20 % RH (α -30,20), (b) and (d) α -pinene + isoprene oxidation products at -30 °C and 20 % RH (α IP-30,20). The level of α -pinene was between 1 and 8 ppbv in (a) (b) (c) and (d), while isoprene level reached up to 30 ppbv in (b) and (d). Ozone level was stable at ~ 100 ppbv for all the experiments. The intensities are normalized by the total signal in each system and phase. Each color represents a specific number of oxygen atoms in the range of 3 to 16.

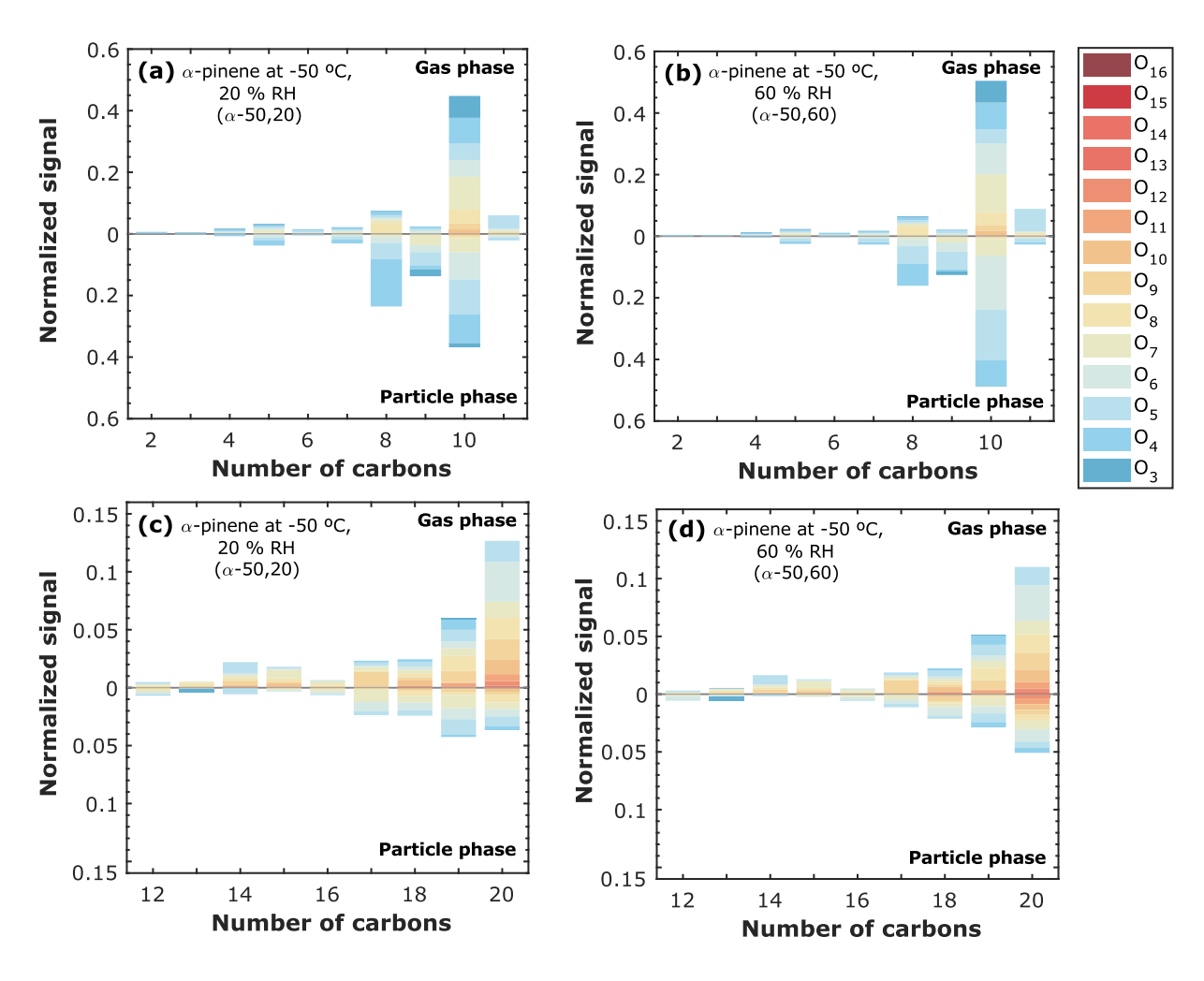


Figure S2. Carbon atom distribution C_{2-11} and C_{12-20} and oxygen atom content in gas and particle phase molecules. Both phases are measured with a Nitrate CI-APi-TOF mass spectrometer, while the TD-DMA is coupled to it for particle phase measurements. (a) and (c) α -pinene oxidation products at -50 °C and 20 % RH (α -50,20), (b) and (d) α -pinene oxidation products at -50 °C and 60 % RH (α -50,60). The level of α -pinene was between 1 and 8 ppbv and Ozone level was stable at ~ 100 ppbv for all the experiments. The intensities are normalized by the total signal in each system and phase. Each color represents a specific number of oxygen atoms in the range of 3 to 16.

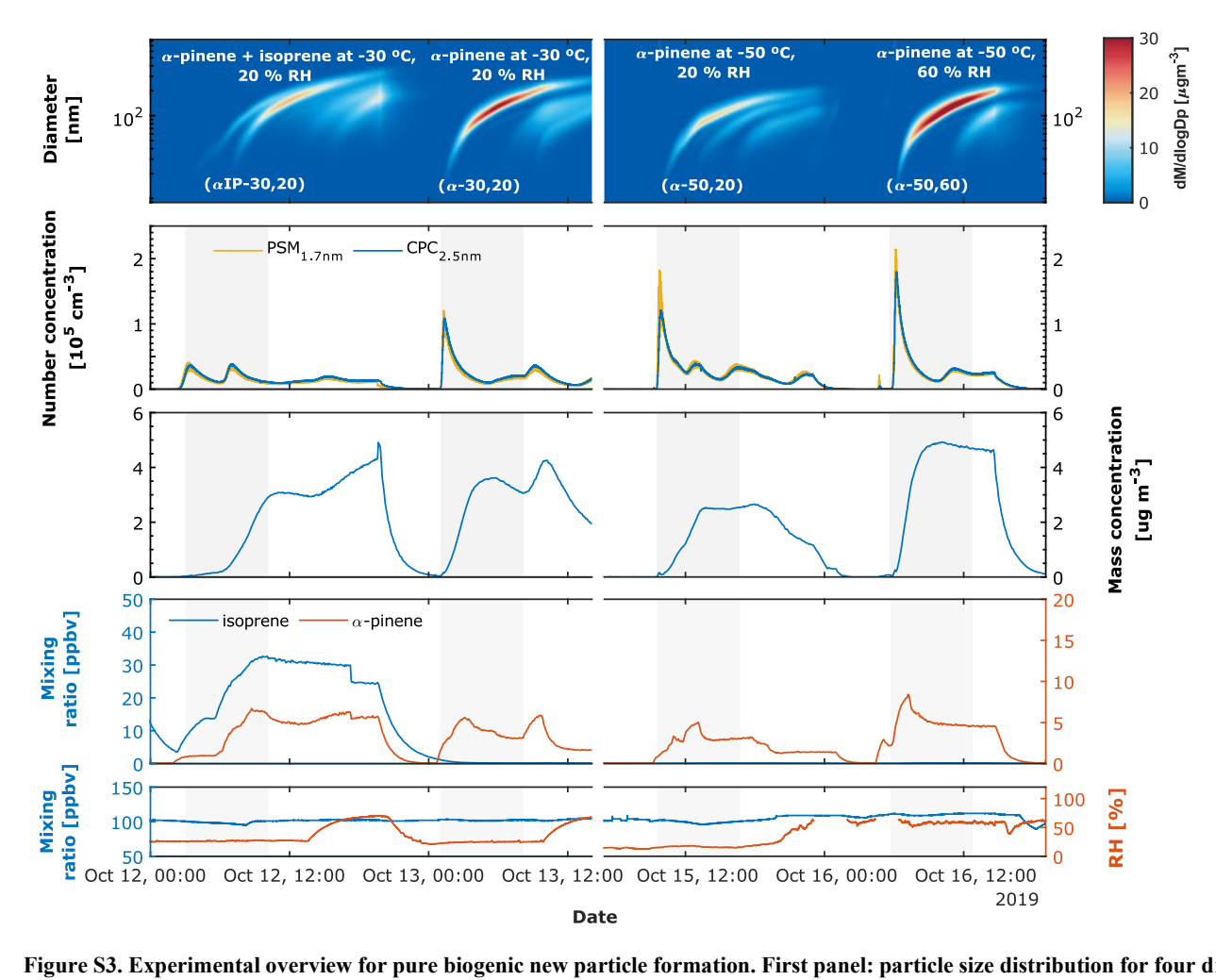


Figure S3. Experimental overview for pure biogenic new particle formation. First panel: particle size distribution for four different experiments: α-pinene + isoprene at -30 °C and 20 % RH (αIP-30,20); α-pinene at -30 °C and 20 % RH (α-30,20); α-pinene at -50 °C and 20 % RH (α-50,20) and α-pinene at -50 °C and 60% RH (α-50,60). The color scale represents the normalized mass concentration in μg m⁻³. Second panel: Particle number concentration in cm⁻³ measured by the PSM with a cut-off diameter of 1.7 nm and CPC with a cut-off diameter of 2.5 nm. Third panel: Mass concentration in μg m⁻³ (obtained by integrating the normalized mass concentration from the SMPS). Fourth panel: Mixing ratio in ppbv for the biogenic precursor gases, isoprene and α-pinene. Fifth panel: Ozone mixing ratio in ppbv and relative humidity in %. The shaded areas refer to the time where the particles were collected using the TD-DMA.

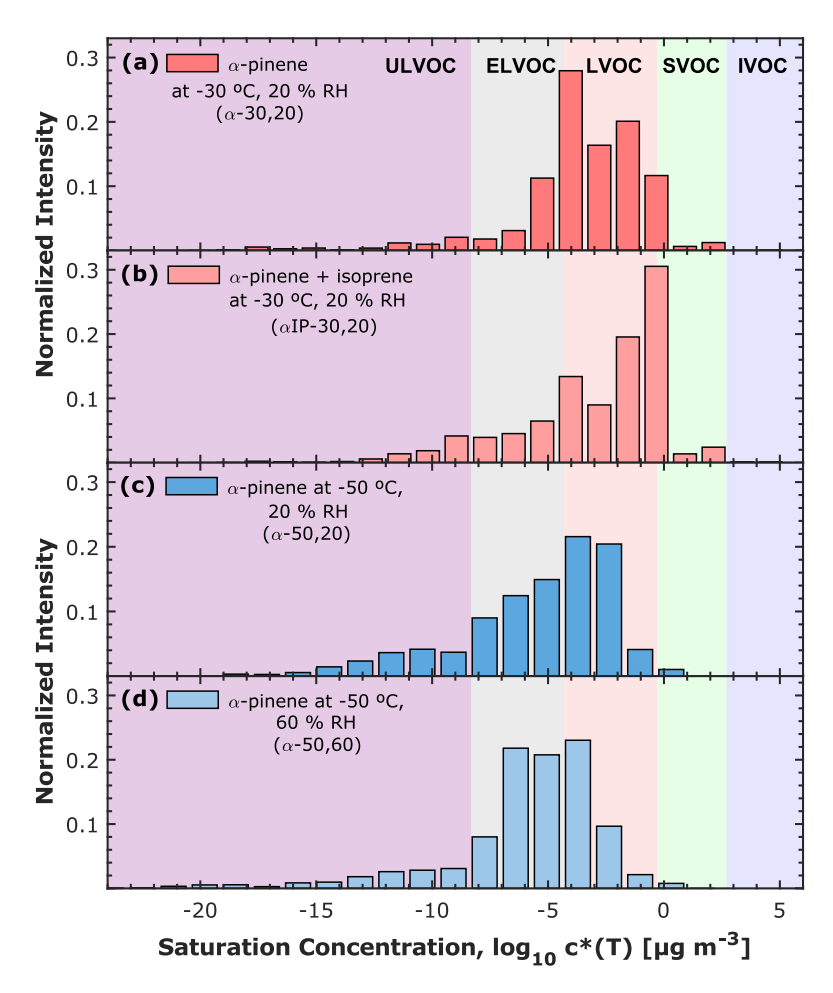
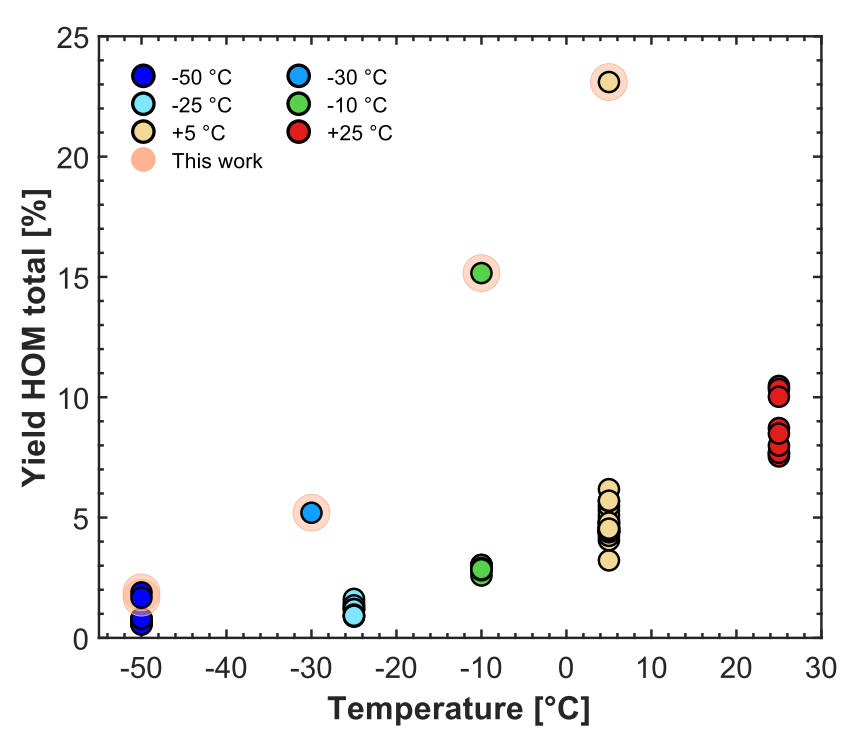


Figure S4. TD-DMA Volatility distribution of the measured oxidation products in the particle phase for four different experiments (Figure 5 in linear scale): (a) α-pinene at -30 °C and 20 % RH (α-30,20); (b) α-pinene + isoprene at -30 °C and 20 % RH (αIP-30,20); (c) α-pinene at -50 °C and 20 % RH (α-50,20) and (d) α-pinene at -50 °C and 60 % RH (α-50,60). Every individual volatility bin includes the sum of the intensity for the oxidation products normalized by the total signal in each system. Every individual volatility bin is defined at 300 K, shifted, and widened according to their corresponding temperature. The color bands in the background indicate the volatility regimes as in Donahue et al. (2012) and in Schervish and Donahue (2020). The normalized intensity is dimensionless. Nevertheless, it should be noted that the particle phase signal is given in normalized counts per second integrated over the evaporation time [ncps. s].



45 Figure S5. Yield of total HOM as a function of temperature for pure α-pinene systems. Data points at -50 °C, -25 °C, -10 °C, +5 °C and +25 °C are from Simon et al. (2020) and the data points with the orange shadows are the contribution of this study (α-30,20, α-50,20 and α-50,60 and complementary pure α-pinene experiments at +5 °C and at -10 °C). The level of precursor gases from Simon et al., (2020) were 0.2 to 0.8 ppbv for α-pinene and 40 to 50 ppbv for ozone, while for experiments reported here (shown with orange shadows), the mixing ratios were 1 to 8 ppbv for α-pinene and 100 ppbv for ozone.

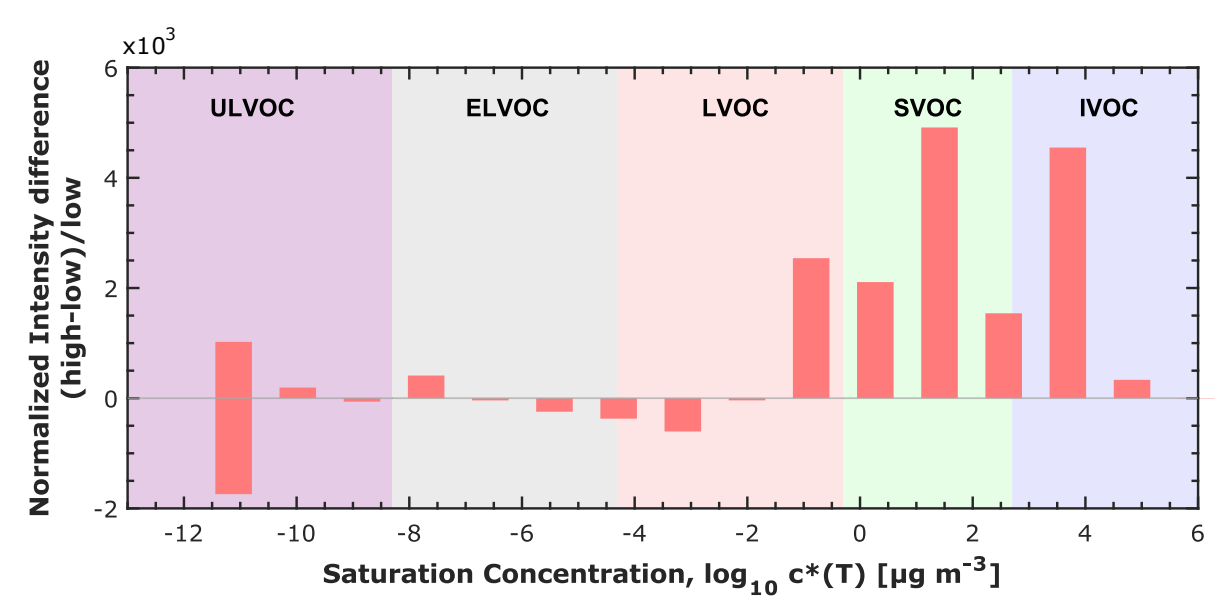


Figure S6. Volatility distribution of gas phase for two different systems and the normalized difference between them. Gas phase is measured with a Nitrate CI-APi-TOF mass spectrometer. Every individual volatility bin includes the normalized intensity difference (high-low)/low, which is calculated based on intensity of the system at high level of precursor gases (α -pinene was 2 - 3 ppbv and Ozone ~ 100 ppbv) and on the system at low level of precursor gases (α -pinene was 0.2 - 0.8 ppbv and Ozone ~ 40 - 50 ppbv). Every individual volatility bin is defined at 300 K, shifted, and widened according to their corresponding temperature. The lowest bin is an overflow bin (which contains the volatility bins with saturation concentration < -11 ug m⁻³.). The color bands in the background indicate the volatility regimes as in Donahue et al. (2012) and in Schervish and Donahue (2020).

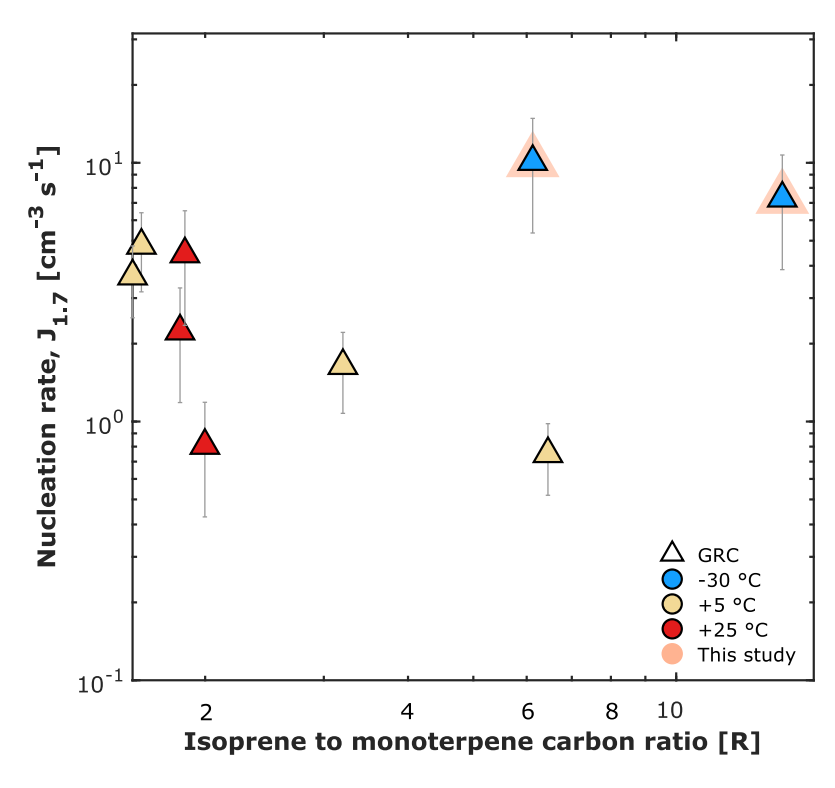


Figure S7. Pure biogenic nucleation rates at 1.7 nm diameter against isoprene-to-monoterpene carbon ratio (R) at different temperatures. Triangles represent Galactic Comic Rays (GCR) conditions. Data points at +5 °C and +25 °C are from Heinritzi et al., (2020). The points with the orange shadows are the experiments reported in this study for α -pinene + isoprene oxidation products at -30 °C and 20 % RH (α IP-30,20).